

5-2014

Winglet Performance Evaluation through the Vortex Lattice Method

Phil R. Rademacher
Embry-Riddle Aeronautical University - Daytona Beach

Follow this and additional works at: <https://commons.erau.edu/edt>



Part of the [Aerospace Engineering Commons](#)

Scholarly Commons Citation

Rademacher, Phil R., "Winglet Performance Evaluation through the Vortex Lattice Method" (2014).
Dissertations and Theses. 178.
<https://commons.erau.edu/edt/178>

This Thesis - Open Access is brought to you for free and open access by Scholarly Commons. It has been accepted for inclusion in Dissertations and Theses by an authorized administrator of Scholarly Commons. For more information, please contact commons@erau.edu.

WINGLET PERFORMANCE EVALUATION THROUGH THE VORTEX LATTICE
METHOD

by

Phil R. Rademacher

A Thesis Submitted to the College of Engineering, Department of Aerospace Engineering
in Partial Fulfillment of the Requirements for the Degree of
Master of Science in Aerospace Engineering

Embry-Riddle Aeronautical University
Daytona Beach, Florida
May 2014


WINGLET PERFORMANCE EVALUATION THROUGH THE VORTEX LATTICE
METHOD


by

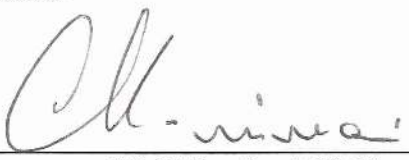
Phil R. Rademacher

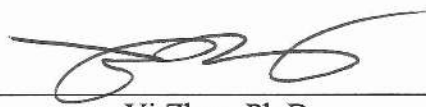
This thesis was prepared under the direction of the candidate's Thesis Committee Chair, Dr. Luis Gonzalez-Linero, Assistant Professor, Daytona Beach Campus, and Thesis Committee Members Snorri Gudmundsson, Assistant Professor, Daytona Beach Campus, and Dr. Maj Mirmirani, Dean – College of Engineering, Daytona Beach Campus, and has been approved by the Thesis Committee. It was submitted to the Department of Aerospace Engineering in partial fulfillment of the requirements for the degree of Master of Science in Aerospace Engineering.

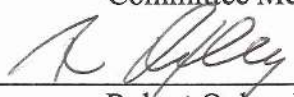
Thesis Review Committee:


Luis Gonzalez-Linero, Ph.D.
Committee Chair


Snorri Gudmundsson, Assist. Prof.
Committee Member


Maj Mirmirani, Ph.D.
Dean of the College of Engineering,
Committee Member


Yi Zhao, Ph.D.
Graduate Program Chair,
Department of Aerospace Engineering


Robert Oxley, Ph.D.
Associate Vice President of Academics

6-3-2014
Date

Acknowledgements

Surviving an ordeal like a Master's thesis is never easy without the help of dedicated individuals. First and foremost I would like to appreciate all the effort Dr. Luis Gonzalez put into my thesis and dealing with the mistakes that he encountered. Prof. Snorri Gudmundsson has been an incredible mentor and shows an unbelievable dedication to his students, Dr. Maj Mirmirani, who despite his busy schedule, always kept track of the project and his willingness on short notice to join the thesis committee. Donald Pointer, who has been incredibly helpful answering or forwarding any type of questions. Lionel De LaSayette for his fun and fresh inputs on problems. Michel Lavanant for the calm and great engineering mind. Pilot Alan Carter and "his" aircraft Juliet Lima for putting my mind at ease when coming up with some new performance numbers.

Of course an undertaking like this has moments when support and distractions are needed and I am really thankful to my mom, dad, and family for supporting me, my friends who made sure I still retained some sort of sanity and social life, the aviation community in general, and most of all, the creations of our profession, the aircraft themselves, which just seeing them gave me energy to finish this work.

Abstract

Researcher: Phil R. Rademacher
Title: Winglet Performance Evaluation through the Vortex Lattice Method
Institution: Embry-Riddle Aeronautical University
Degree: Master of Science in Aerospace Engineering
Year: 2014

The purpose of the study was to assess the possibility of retrofitting winglets to the Dassault Falcon 10 small size business jet using the vortex lattice method solver program SURFACES© by GreatOWL Publishing. The winglet geometric parameters investigated were the winglet span, cant angle, sweep and taper ratio in terms of their influence on drag, range, fuel burn, as well as wing root bending moments. The results of the research show that winglet span and cant angle offer the highest gains in terms of performance while taper ratio and sweep angle have a minor contribution. In general, all winglets provided an increase in aerodynamic efficiency, however, certain configurations result in wing root bending moments and weight increases that would make a retrofit option impractical.

Table of Contents

	Page
Thesis Review Committee	ii
Acknowledgements	iii
Abstract	iv
List of Tables.....	vi
List of Figures	vii
Definition of Terms	ix
List of Acronyms	ix
Chapter	
I Introduction	1
1.1 Statement of the Problem.....	1
1.2 Study Statement.....	1
1.3 Significance of the Study.....	2
1.4 Scope of Study	3
1.5 Limitations and Assumptions.....	4
II Review of the Relevant Literature	5
2.1 History of winglet research.....	5
2.1.1 Whitcomb’s Groundbreaking Research	5
2.1.2 KC-135 Winglet Flight Test.....	7
2.1.3 Wingtip Devices Today.....	7
2.2 Benefits and Drawbacks of Winglets	9
2.2.1 Benefits	9

	2.2.2 Drawbacks	9
III	Methodology	11
	3.1 Research Approach.....	11
	3.2 Model Geometry	12
	3.2.1 Baseline Model	12
	3.2.2 Model with Wing Extensions	13
	3.3 Drag Model	14
	3.3.1 Parasitic Drag due to Winglets	15
	3.3.2 Induced Drag	17
	3.3.3 Wave Drag.....	17
	3.4 Calibration of SURFACES©	19
	3.4.1 Drag Correction to Include Separation Effects	21
	3.5 Panel Sensitivity	21
	3.6 Range Analysis.....	22
	3.6.1 Wing Root Bending Moments.....	22
	3.6.2 Winglet Weight	22
	3.6.3 Climb Segment	23
	3.6.4 Cruise Segment.....	24
	3.6.5 Fuel Consumption and Savings	25
IV	Results and Discussion	26
	4.1 Effect of Winglet Configurations on Total Aircraft Drag	26
	4.2 Winglet Weight	28
	4.3 Wing Root Bending Moment Analysis	29

4.4	Range Analysis.....	31
4.5	Fuel Savings.....	34
V	Conclusion and Recommendations	38
5.1	General Observations	38
5.2	Conclusion	38
	5.2.1 Recommended Winglet Shape for Detailed Research	40
5.3	Recommendations for Future Research.....	42
	References.....	43
	Bibliography.....	45
	Appendices	
A	Climb Performance Analysis Process	48
B	Cruise Performance Analysis Process	52
C	SURFACES© Validation Examples	54

List of Tables

Table	Page
3.1 List of Winglet Parameters	14
3.2 Typical Interference Factors	15
4.1 Fuel Saved per Nautical Mile	15
4.2 US-Dollar Savings per Nautical Mile	36
4.3 Cost savings for b25Γ675Λ225λ25	37

List of Figures

Figure	Page
1.1 Dassault Falcon 10.....	2
2.1 Aerodynamic Effect of Winglet.....	6
2.2 Selected Winglet Configurations	8
3.1 SURFACES© Baseline Model.....	12
3.2 Winglet Geometry and Dimensions.....	13
3.3 Comparison of Wind Tunnel Data to Wave Drag Equation	19
3.4 C_L vs α Comparison.....	20
3.5 C_D vs α Comparison.....	20
3.6 L/D vs α Comparison.....	20
3.7 Selected Panel Sensitivity Results	21
3.8 TFE731-2 Maximum Continuous Thrust and TSFC vs Altitude and Mach Number.....	24
3.9 TFE731-2 TSFC vs Thrust	25
4.1 Change in Drag Coefficient with Focus on Break-Even Point.....	27
4.2 Improvement in Lift-to-Drag Ratio	28
4.3 Projected Winglet Installation Weights	28
4.4 Root Bending Moment Ratio between Winglet and Baseline Aircraft.....	30
4.5 Range Increase over Baseline Aircraft for Mach 0.70 Cruise Speed	31
4.6 Range Increase over Baseline Aircraft for Mach 0.80 Cruise Speed	32
4.7 Range Increase over Baseline Aircraft for Mach 0.84 Cruise Speed	32
5.1 Dassault Falcon 10RX and 10LX	41

<i>C.1</i>	SURFACES© Validation Example 1	54
<i>C.2</i>	SURFACES© Validation Example 2	55
<i>C.3</i>	SURFACES© Validation Example 3	55

Definitions of Terms

Cant Angle between the vertical and the winglet

Dihedral Definition including citation, as needed.

Toe-in/-out Angle of incidence of the winglet if viewed from above.

Wing Root Bending Moment Moment created along the x-axis located at the wing root by the lift forces acting on the wing.

List of Acronyms

AOA	Angle of Attack
ERAU	Embry-Riddle Aeronautical University
FAA	Federal Aviation Administration
KCAS	Knots Calibrated Airspeed
KTAS	Knots True Airspeed
MTOW	Maximum Take-Off Weight
NASA	National Aeronautics and Space Administration
NWL	No Winglet (Depicting Baseline Aircraft)
USAF	United States Air Force
PBT	Prandtl-Betz-Trefftz Plane
RoC	Rate-Of-Climb
SSL	Standard Sea Level
TSFC	Thrust Specific Fuel Consumption
VLM	Vortex Lattice Method
WL	Winglet
AR	Aspect Ratio

b	Wingspan
M	Mach Number
M_0	Maximum Mach Number at Sea Level
M_{crit}	Critical Mach Number
M_{maxD}	Mach Number where $\Delta C_{D_{maxD}}$ occurs
\bar{c}_{WL}	Reference Chord Length of Winglet
C_D	Drag Coefficient
C_{D_f}	Skin Friction Drag Coefficient
$C_{D0_{new}}$	New Minimum Drag for Modified Aircraft
$C_{D0_{old}}$	Original Minimum Drag for Unmodified Aircraft
$C_{D0_{old+wave}}$	Original Minimum Drag plus Wave Drag for Unmodified Aircraft
C_{D_i}	Induced Drag Coefficient
$C_{f_{urb}}$	Skin Friction Coefficient
$C_{f_{turb}}$	Turbulent Skin Friction Coefficient
C_L	Lift Coefficient
$C_{L_{min D}}$	Lift Coefficient at Minimum Drag
ΔC_D	Drag Difference Function between Wind Tunnel and SURFACES©
$\Delta C_{D_{WL}}$	Drag Increase from Winglet
ΔC_{D_M}	Additional Drag due to Compressibility Effects (Wave Drag)

$\Delta C_{D_{maxD}}$	Maximum Drag due to Mach Drag Divergence
D	Drag Force
FF	Form Factor
IF	Interference Factor
L	Lift Force
L_{WL}	Lift Force on Winglets
e	Span Efficiency
h	Altitude
\dot{m}	Mass Flow (Fuel Consumed)
n_z	Ultimate Load Factor
Re	Reynold's Number
q	Dynamic Pressure
S_{WL}	Winglet Surface Area
S_{wet_WL}	Wetted Surface Area of Winglet
S_{ref}	Reference Wing Area
t	Time
T	Thrust Force
$\frac{t}{c}$	Thickness-to-Chord Ratio of an Airfoil
V_A	Maximum Maneuvering Airspeed
V_{TAS}	True Airspeed in feet per second
V_V	Rate-Of-Climb (Vertical Airspeed)

W	Aircraft Weight
W_0	Maximum Design Weight (usually MTOW)
W_{ZFW}	Zero-Fuel Weight
W_{TOC}	Weight at Top-Of-Climb
W_{TOD}	Weight at Top-Of-Descend
W_{WL}	Winglet Weight
Γ	Cant Angle
$\Lambda_{c/2}$	Sweep Angle at Half Chord
$\Lambda_{c/4}$	Sweep Angle at Quarter Chord
λ	Taper Ratio
μ	Air Viscosity
ρ	Air Density
σ	Air Density Ratio

Chapter I

Introduction

Looking at airports these days, it usually does not take long to spot at least one or more aircraft that feature what looks like a set of nearly vertical, wing-like surfaces attached to the wingtips. These so called winglets have been a remarkable invention to increase the efficiency of aircraft by substantially reducing drag coefficients at lifting conditions (Whitcomb, 1976). Newer as well as older aircraft designs often feature winglets nowadays, due to their advantages. For older aircraft, winglets are often retrofitted because they are a comparatively cost effective choice when evaluated against other upgrades, such as new engines.

1.1 Statement of the Problem

Retrofitting winglets to an existing airframe has to be a viable option for a manufacturer. Providing such an upgrade for older aircraft types has to show a significant increase in performance, efficiency, or market value to the aircraft owner to consider the upgrade; however, installing a poorly designed winglet configuration could result in a marginal performance increase at best or even in an overall performance reduction (Whitcomb, 1976). It is therefore in the best interest of a manufacturer to determine in the preliminary aerodynamic analysis which configurations offer the highest benefits and whether they warrant further studies.

1.2 Study Statement

The purpose of this study is to perform a preliminary aerodynamic investigation of several winglet geometric configurations for use as a retrofit on a small cabin size

business jet; namely the Dassault Falcon 10 pictured in Figure 1.1 to determine their impact on the range, fuel saved, wing root bending moments, and weight increase in order to select a single winglet configuration as a possible retrofit option.



Figure 1.1. Dassault Falcon 10. 226 Falcon 10 and Falcon 100 were produced between 1973 and 1989 (Dassault Aviation, 2013) (Picture by author).

1.3 Significance of the Study

The development of new components for an old aircraft design is always a question of proportionality. A business jet like the Dassault Falcon 10 that has been in service for nearly thirty years is now closer to its retirement. With this in mind, minimizing the resources allocated to develop new content is important in order to keep

the final cost associated with an upgrade low and give the owners a tangible benefit. Utilizing a vortex lattice method (VLM) code helps find the optimum winglet parameters for a performance increase in a reasonable timeframe and for a low cost.

1.4 Scope of Study

The main scope of the research was to study how several winglet geometric parameters affect the cruise performance of the Dassault Falcon 10 business jet. The parameters evaluated were the winglet span, cant and sweep angles, and taper ratio. Different combinations were assessed in terms of range increase and fuel burn for climb and typical cruise conditions of Mach speeds of 0.70, 0.80, and 0.84 at 35,000ft.

Another important parameter analyzed was the reduction in the drag coefficient from the installation of winglets. The added parasitic drag from the winglets was calculated by empirical formulas, while the reduction in induced drag was evaluated by the VLM program using a Prandtl-Betz-Trefftz (PBT) plane.

Furthermore, while structural aspects were not covered, the root bending moments were included in the analysis to produce a realistic assessment of which winglet configuration would be the most likely candidate for further in-depth studies in a Falcon 10 winglet retrofit program. These moments were calculated using the design maneuvering speed V_A at limit load factor as the evaluation point in SURFACES©. Finally, a simple winglet weight estimation was carried out, using the empirical wing weight equation given by Nicolai (Nicolai & Carichner, 2010).

1.5 Limitations and Assumptions

For simplicity, the winglets used in this study had the same airfoil as the original wingtip. For the toe-out angle, the tip wash-out angle was selected, so that there was no difference between the winglets, ensuring similar stall characteristics to those of the original aircraft, especially for the horizontal tip extensions.

VLM codes provide fast solving capabilities that allow for an easy exploration of a large number of design cases, but by the nature of the method they do not include viscous effects nor compressibility drag and are incapable of predicting flow separation. For this reason empirical corrections based on wind tunnel data were included, assuming that the increase in drag coefficient at higher angles of attack for the aircraft with winglets was similar to that of the wind tunnel baseline model. Compressibility effects were accounted for by assuming that the wave drag of the aircraft with winglets would be the same as that of the wind tunnel baseline model. Additionally, a fully turbulent boundary layer was assumed for the parasitic drag calculations.

For the assessment of the impact on the aircraft range, keeping the maximum take-off weight (MTOW) and the maximum fuel capacity unchanged, the winglet weight was subtracted from the fuel weight to evaluate the aircraft at the same payload mission.

In this study only the wing root bending moment increase was addressed and not any other structural issues, like, for example, flutter characteristics, which were considered beyond the scope of this thesis.

Chapter II

Review of the Relevant Literature

2.1 History of Winglet Research

The first ideas of adding vertical endplates to the wingtips for a reduction in induced drag were first proposed in the early 20th century; however, they failed because their increase in profile drag outweighed any induced drag reductions (McLean, 2005). In 1976 Richard T. Whitcomb demonstrated that a net gain in drag reduction through non-planar wingtip extensions was possible “through good aerodynamic design practice” (McLean, 2005). The results of his investigations together with the 1970s fuel crisis encouraged aircraft manufacturers to explore the benefits of incorporating winglets into designs. Gates Learjet was one of the first companies to put winglets on a production aircraft, the Gates Learjet 28/29 Longhorn (Gudmundsson, 2014). Since then the amount of aircraft featuring winglets and other wingtip devices have increased rapidly.

2.1.1 *Whitcomb’s Groundbreaking Research*

Whitcomb’s paper on wing-tip mounted winglets can be seen as the starting point for the success of winglets. In his 1976 paper *A Design Approach and Selected Wind-Tunnel Results at High Subsonic Speeds for Wing-Tip Mounted Winglets* he found several key factors that are presented in the following paragraphs.

For a vertical wingtip surface to positively contribute to the aircraft's performance, it has to produce significant side forces (Whitcomb, 1976). If they also generate some forward force component it will add to the thrust of the aircraft as shown in Figure 2.1, with an effect similar to sailing boats tacking upwind (Barber, et al., 1981).

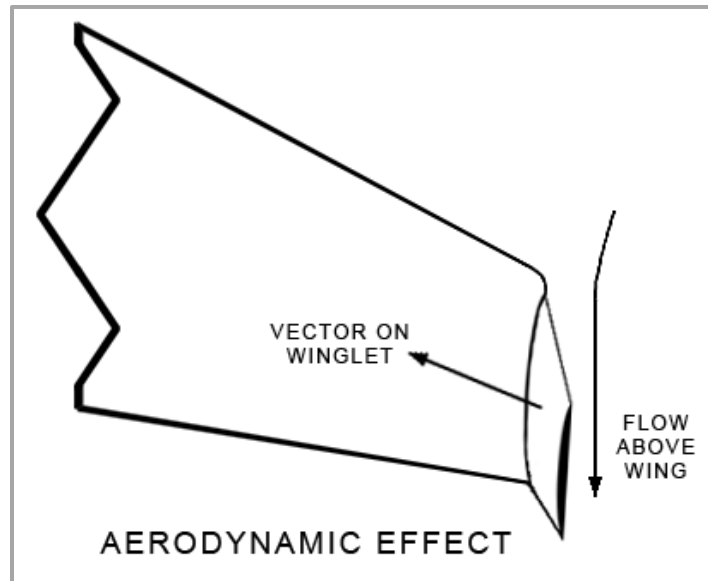


Figure 2.1. Aerodynamic Effect of Winglet. The illustration shows the forward lift contribution of the Whitcomb winglet – modified from (Barber, et al., 1981).

Previous low-aspect ratio flat end plates were producing only small, if any, side forces and for that reason did not yield a net gain in drag reductions. Whitcomb recommends certain geometries that result in an effective net drag reduction, namely, that the sweep of the winglet should be approximately the same as that of the main wing. A substantial taper ratio is recommended to achieve an approximately constant normal force coefficient. The airfoil should be chosen in a way that achieves the desired inward normal-force coefficients at the design conditions, avoiding strong shockwaves in supercritical conditions and the pressure distribution should delay the boundary layer

separation on the winglet after flow separation appears on the main wing. To provide an inward direction of the normal force the winglet should be positioned with a toe-out angle. Twist is generally not required for a winglet.

Finally, based on theoretical calculations by Lundry (Lundry, 1968), Whitcomb articulates that a practical winglet configuration should have at least a small amount of outward cant.

The wind tunnel results showed that his winglet design would reduce induced drag by 20 % and increase the lift-to-drag ratio by 9 % (Whitcomb, 1976). Another interesting observation was that toe-out incidence angles larger than 4° significantly increased bending moments as well as drag coefficients, therefore leading to the conclusion that large toe-out angles could be detrimental to the winglet performance (Whitcomb, 1976).

2.1.2 KC-135 Winglet Flight Test

Boeing and the United States Air Force conducted a joint research program to retrofit a Boeing KC-135A Stratotanker with removable winglets. They compared wind tunnel results with actual flight test data and evaluated the benefits of winglets on a real aircraft (Barber, et al., 1981). The wind tunnel results were verified and improvements in fuel mileage between 4.4 % and 7.2 % were demonstrated (Barber, et al., 1981).

2.1.3 Wingtip Devices Today

Modern day aircraft feature a variety of winglet designs, with some examples shown in Figure 2.2. Each configuration offers advantages and disadvantages, not only limited to aerodynamic factors, but also to structural, flutter and cost requirements. The

most common winglet shapes seen on aircraft today are the blended winglet shown in Figure 2.2e and the simple winglet shown in Figure 2.2f. The blended winglet has the advantage of having a smoother transition between wing and winglet that optimizes the span load lift distribution and helps minimize negative interference effects (Faye et al., 2002).

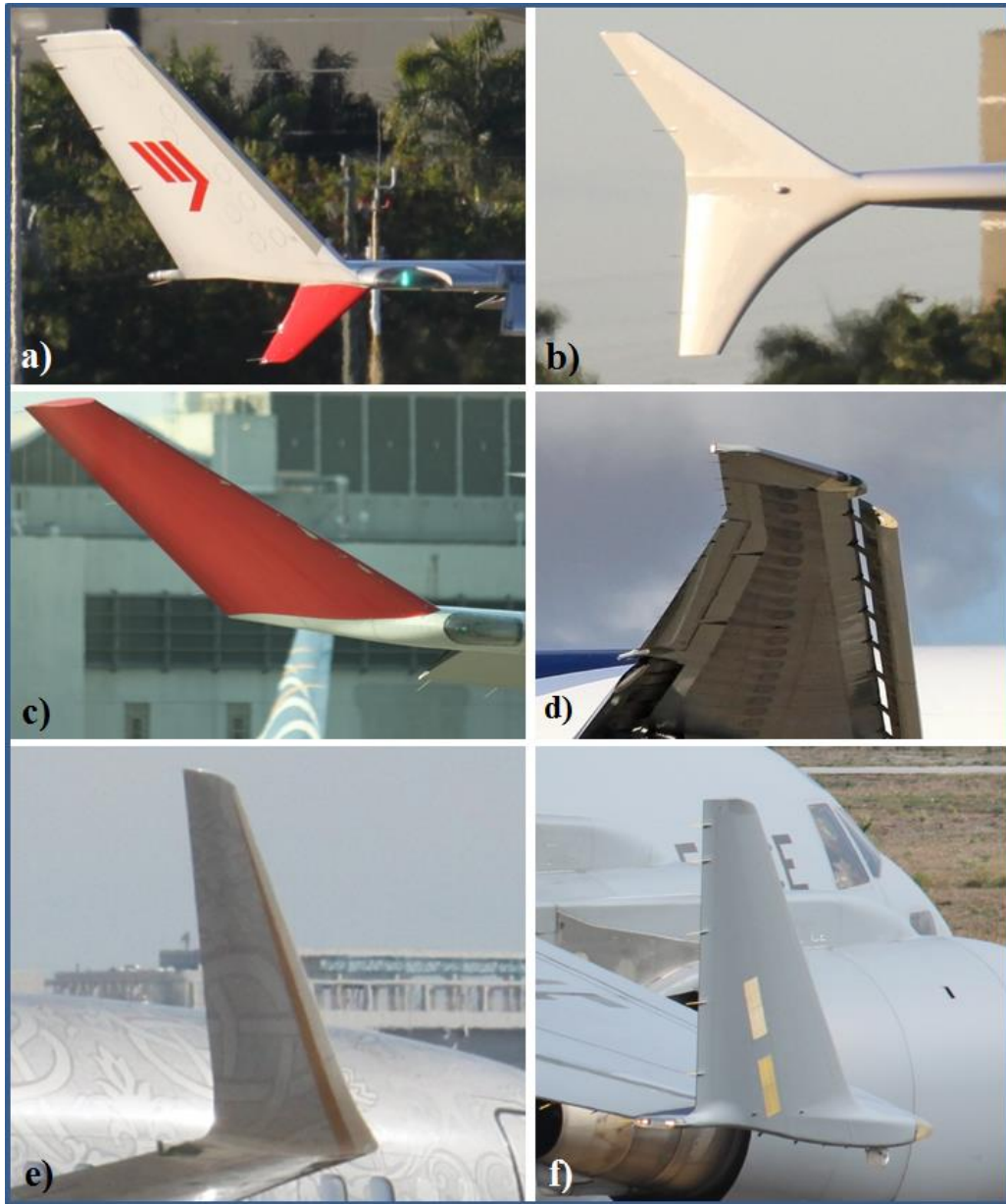


Figure 2.2. Selected Winglet Configurations. a) Whitcomb Winglet (McDonnell-Douglas MD-11), b) Wingtip Fence (Airbus A380), c) Canted Winglet (Airbus A330), d)

Raked Wingtip (Boeing 777F), e) Blended Winglet (Boeing 737), f) Simple Winglet (Boeing C-17A Globemaster III) (Pictures by author).

2.2 Benefits and Drawbacks of Winglets

The basic purpose of a wing extension of any kind is to increase the effective aspect ratio of the wing (Heyson, Riebe, & Fulton, 1977). Lowering the AOA reduces the wingtip vortices, and therefore the induced drag (Gudmundsson, 2014) as shown in the induced drag equation,

$$C_{Di} = \frac{C_L^2}{\pi \cdot AR \cdot e} \quad (2.1)$$

Where

C_L : Lift Coefficient

AR : Aspect Ratio

e : Span Efficiency

2.2.1 Benefits

Designed correctly, winglets reduce induced drag at climb and cruise, which translates into lower fuel burn, increased range, shortened take-off field length, higher cruise altitude and cruise speed, and reduced take-off noise. All these improvements can come without significant increase in wingspan, which can be a limiting factor on airports. Finally, they provide a subjective esthetic improvement (McLean, 2005).

2.2.2 Drawbacks

There are several drawbacks that have to be addressed, namely:

1. Drag: Winglets increase profile drag due to the additional wetted area and possible interference flow between wing and winglet.
2. Weight: The empty weight of the aircraft is increased due to the winglet itself and the installation of attachment fittings.
3. Structural changes: The attachment of winglets and the increase in wing bending moments may require substantial wing structural reinforcements.
4. Flutter: The higher weight at the tip from the winglet as well as structural modifications can have a negative impact on the flutter and fatigue characteristics of the aircraft by reducing the natural frequency of the wing.
5. Stability: The winglet cant effectively increases the dihedral effect of the wing, therefore changing the stability of the aircraft. Also, a vertical winglet adds additional side area to the aircraft upon which a crosswind during landing can act, potentially decreasing the maximum crosswind limit of the aircraft (Gudmundsson, 2014, McLean, 2005).

Chapter III

Methodology

3.1 Research Approach

Vortex Lattice Method based programs can efficiently compute pressure distributions and therefore lift and associated phenomena like induced drag. These advantages make VLM programs ideal for quick turnaround studies in preliminary design. In this research the VLM program SURFACES© was used. Several validation examples from the SURFACES© user manual can be found in Appendix C.

For this study, the baseline aircraft was modeled and calibrated using Falcon 10 wind tunnel data. Once the baseline model was calibrated, panels representing the different winglet configurations were added. For this investigation the winglet geometric factors such as span, cant and sweep angles, and taper ratio were systematically varied. The increase in parasitic drag was accounted for with empirical drag equations that include the geometrical plus the wave drag effects.

Each modification was run at three different Mach speeds to obtain all the necessary coefficients to determine the improvements in lift, drag, range, and fuel efficiency with respect to the baseline aircraft (non-winglet). The wing root bending moment change induced by the winglet was evaluated since it is an indication of the structural modifications that would be needed and thus of the increase in weight.

Throughout the thesis the configurations studied are identified using the following convention $b\#\Gamma\#\Lambda\#\lambda\#$, where b stands for winglet span, Γ for the cant angle, Λ for

sweep, and λ for taper ratio, as referenced in Figure 3.2. For example, the winglet with a 3.5 ft. span, 67.5° cant, 22.5° sweep, and a taper ratio of 0.50 would be b35 Γ 675 Λ 225 λ 5.

3.2 Model Geometry

3.2.1 Baseline Model

Figure 3.1 shows the baseline model in SURFACES[©]. The wing panels include the geometrical data of the four airfoils used in the Falcon 10. The model does not include the horizontal stabilizer since it was calibrated against the “tail-off” wind tunnel model.

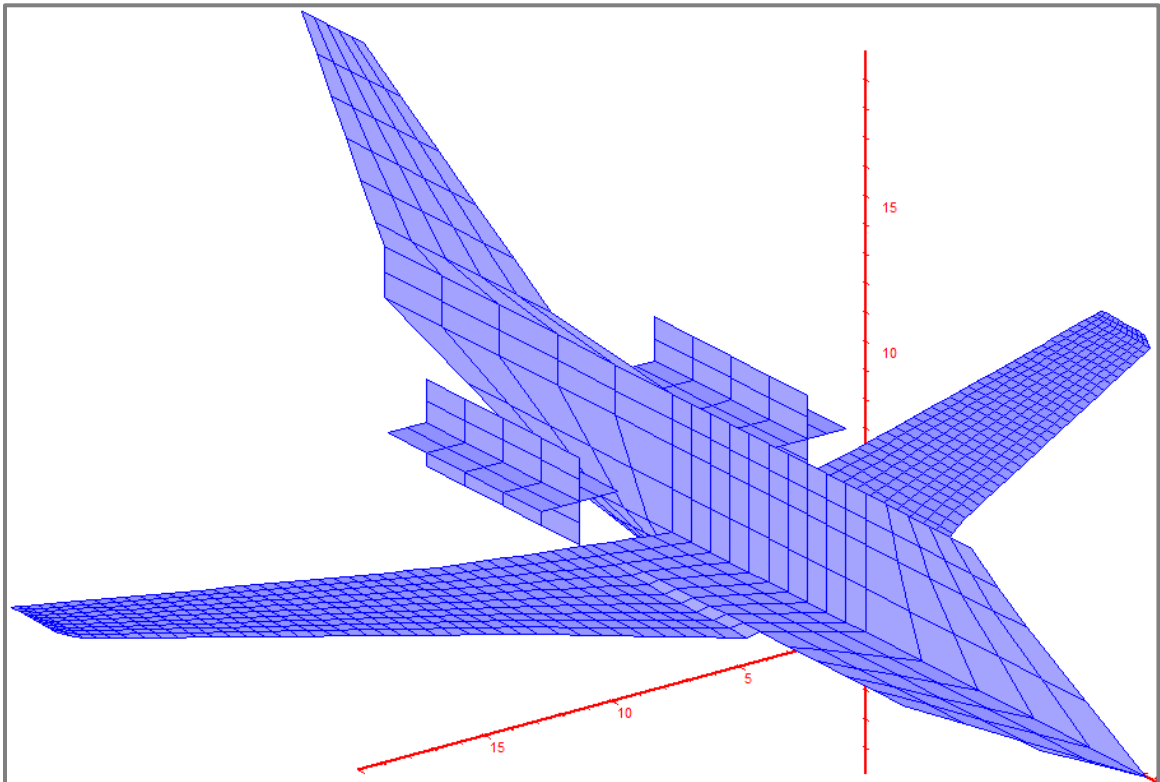


Figure 3.1. SURFACES[©] Baseline Model. This model represents the configuration tested in the wind tunnel which did not include a horizontal stabilizer.

3.2.2 Model with Wing Extensions

Most aircraft today feature only an upper winglet because the additional lower surface of the original Whitcomb winglet (Figure 2.2a), with the geometrical constraints imposed by practical considerations did not improve the performance noticeably (Whitcomb, 1976) (Gudmundsson, 2014). Therefore, it was decided to retain only the upper winglet form with the general parameters described in Figure 3.2.

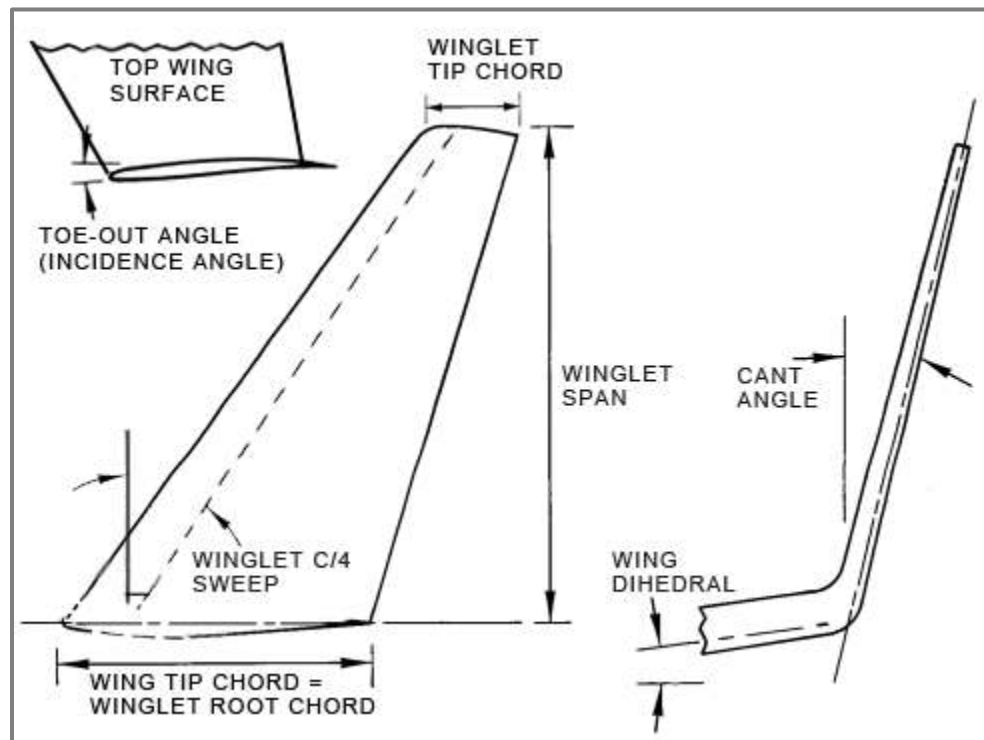


Figure 3.2. Winglet Geometry and Dimensions. Descriptive schematic showing the general measurements of a winglet – modified from Whitcomb’s report (Whitcomb, 1976).

The different configurations were created by extending the wingspan, increasing the quarter chord sweep angle by 22.5° and 45° , modifying the winglet wingtips to obtain taper ratios of either 0.25 or 0.50 and varying the cant angle from 90° (planar extension)

to 5° in 22.5° increments. The winglets studied in this thesis are the results of all the permutations of the parameters presented in Table 3.1.

Table 3.1

List of Winglet Parameters. Overview of winglet parameter that were studied: winglet span b , cant angle Γ , quarter chord sweep angle $\Lambda_{c/4}$, and taper ratio λ .

Γ	90.0°	67.5°	45.0°	22.5°	5.0°
b	2.0 ft.	2.5 ft.	3.0 ft.	3.5 ft.	4.0 ft.
$\Lambda_{c/4}$	22.5°	45.0°			
λ	0.25	0.50			

For the incidence angle, the baseline wingtip wash-out angle of -2° was retained. This value is lower than -4° that Whitcomb mentions as a limit beyond which the winglet would start exhibiting unfavorable effects on bending and drag properties.

3.3 Drag Model

To compute the total drag of the aircraft with winglets, the parasitic drag was calculated with conventional empirical equations, the induced drag was evaluated by SURFACES© using a PBT plane, and the wave drag was accounted for by correction factors derived from wind tunnel data.

3.3.1 Parasitic Drag due to Winglets

The additional drag of the winglets, $\Delta C_{D_{WL}}$, was based on a common formulation, given by equation (3.1) (Gudmundsson, 2014). For this research an interference factor of 1.01 was used, assuming a smooth transition between wing and winglet. The factor of two is used to give the total aircraft drag increase.

$$\Delta C_{D_{WL}} = 2 \cdot FF \cdot IF \cdot C_{f_{urb}} \frac{S_{wet_{WL}}}{S_{ref}} \quad (3.1)$$

Where:

FF : Form factor (calculated by equation (3.2))

IF : Interference factor (based on Table 3.2)

$C_{f_{urb}}$: Skin friction coefficient (calculated by equation (3.3))

$S_{wet_{WL}}$: Winglet wetted surface area [ft²]

S_{ref} : Reference wing area of baseline aircraft [ft²]

Table 3.2

Typical Interference Factors (Gudmundsson, 2014).

Component	Interference Factor (IF)
Whitcomb winglet	1.04
“Airbus” style winglet	1.04
Modern blended winglet	1.0 – 1.01

The form factor, FF , for the wing extension, which takes into account compressibility effects and sweep effects, was based on an equation by Shevell (Gudmundsson, 2014).

$$FF = 1 + \frac{(2 - M^2) \cos(\Lambda_{c/4})}{\sqrt{1 - M^2 \cos(\Lambda_{c/4})}} \left(\frac{t}{c}\right) + 100 \left(\frac{t}{c}\right)^4 \quad (3.2)$$

Where:

M : Mach number

$\Lambda_{c/4}$: Sweep at quarter chord of the surface

$\frac{t}{c}$: Thickness-to-chord ratio of the airfoil

The turbulent flow skin friction coefficient, $C_{f_{urb}}$, was found by means of a variation of the Schlichting relation (Gudmundsson, 2014). The winglet specific Reynolds number Re_{WL} was calculated at the winglet mean geometric chord, \bar{c}_{WL} .

$$C_{f_{urb}} = \frac{0.455}{(\log_{10} Re_{WL})^{2.58} (1 + 0.144M^2)^{0.65}} \quad (3.3)$$

Thus the total minimum drag of the modified aircraft was given by:

$$C_{D0_{new}} = C_{D0_{old+wave}} + \Delta C_{D_{WL}} = (C_{D0_{old}} + C_{D_M}) + \Delta C_{D_{WL}} \quad (3.4)$$

Where:

$C_{D0_{old+wave}}$: Original Minimum Drag from unmodified aircraft including wave drag (calculated by equation (3.8))

$C_{D0_{old}}$: Original Minimum Drag from unmodified aircraft excluding wave drag

3.3.2 *Induced Drag*

The induced drag coefficient is directly calculated by SURFACES©, using the PBT plane vorticity integration. The PBT plane was located 25 wingspans behind the model and contained about 25,200 elements (i.e. the element size was 0.005 wingspans). Using an elliptical wing to tune SURFACES©' calculations, a PBT correction factor of 1.2038 was found.

A mesh sensitivity study was conducted which showed acceptable results with the 25,200 element mesh.

3.3.3 *Wave Drag*

VLM codes do not evaluate wave drag thus empirical corrections were incorporated. The following formulation was utilized (Gudmundsson, 2014)

$$\Delta C_{D_M} = \frac{\Delta C_{D_{maxD}}}{2} (1 + \tanh(A \cdot M + B)) \quad (3.5)$$

Where:

$$A = \frac{\tanh^{-1}\left(\frac{2\Delta C_{DmaxD} - 0.0002}{\Delta C_{DmaxD}} - 1\right) - \tanh^{-1}\left(\frac{0.0002}{\Delta C_{DmaxD}} - 1\right)}{M_{maxD} - M_{crit}} \quad (3.6)$$

and

$$B = \tanh^{-1}\left(\frac{0.0002}{\Delta C_{DmaxD}} - 1\right) - A \cdot M_{crit} \quad (3.7)$$

Where:

ΔC_{DmaxD} : Maximum drag due to Mach drag divergence

M_{maxD} : Mach number at which ΔC_{DmaxD} occurs

M_{crit} : Critical Mach number

The application of the method required the parameters M_{crit} , M_{maxD} , and ΔC_{DmaxD} to be varied to fit the wind tunnel data. This was because these values were not readily definable from the wind tunnel data. The values used were:

$$M_{crit} = 0.74$$

$$M_{maxD} = 1.11$$

$$\Delta C_{DmaxD} = 0.065$$

Giving:

$$\Delta C_{D_M} = \frac{0.065}{2} (1 + \tanh(17.50117M - 16.1886)) \quad (3.8)$$

As evident in Figure.3.3, which shows the resulting $\Delta C_{D_M} + C_{D_{0_{old}}}$, the expression provides a good fit to the wind tunnel data and is thus considered acceptable to estimate wave drag between the experimental data points.

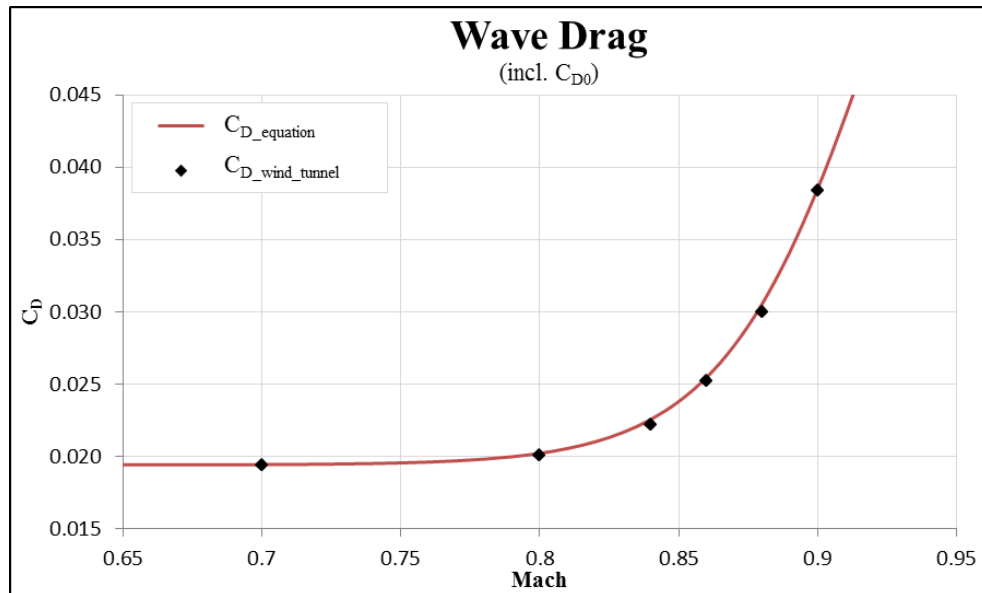


Figure.3.3. Comparison of Wind Tunnel Data to Wave Drag Equation.

3.4 Calibration of SURFACES©

The SURFACES© model was calibrated with respect to the wind tunnel data. The results of the calibration for Mach 0.70 are shown in Figure 3.4, Figure 3.5, and Figure 3.6. A limitation of the inviscid analysis is evident in those three figures, in that it deviates from experiment at high AOA and lift coefficients. However, this is not an issue as the winglets are designed for a flight regime where the data match is acceptable close.

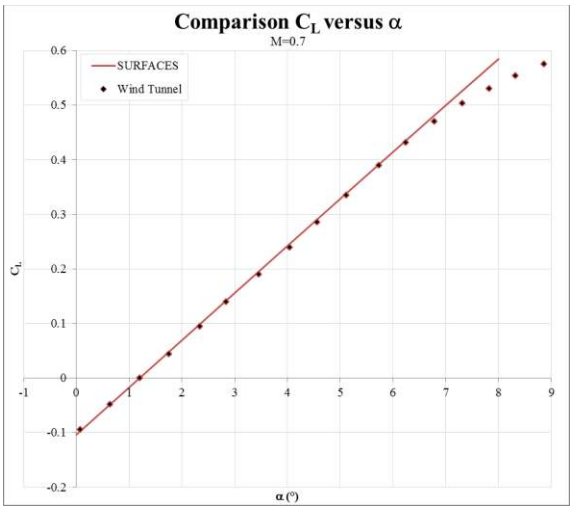


Figure 3.4. C_L vs α Comparison.
Comparison of SURFACES© results with wind tunnel data.

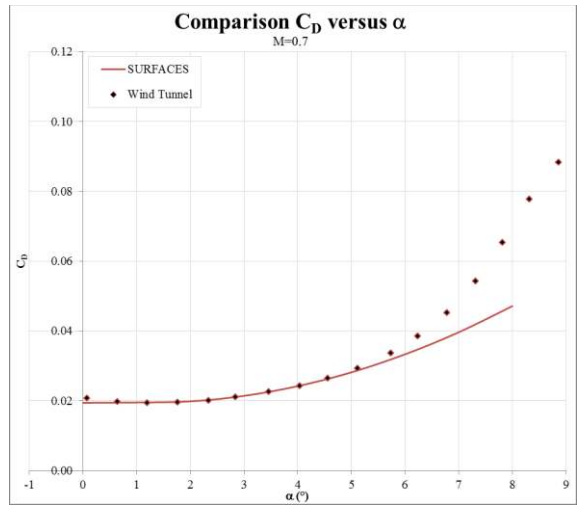


Figure 3.5. C_D vs α Comparison.
Comparison of SURFACES© results with wind tunnel data.

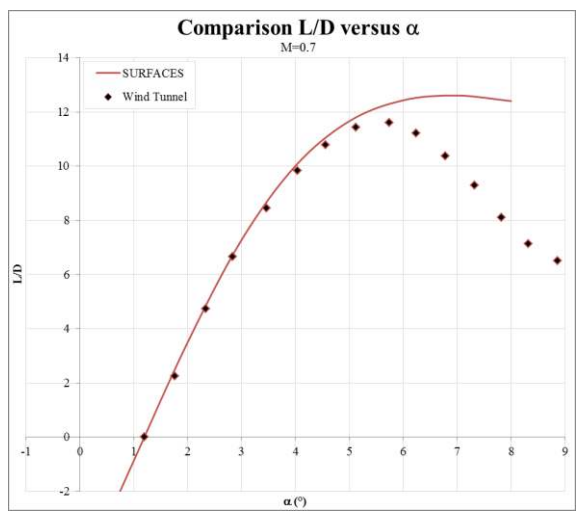


Figure 3.6. L/D vs α Comparison.
Comparison of SURFACES© results with wind tunnel data.

3.4.1 Drag Correction to Include Separation Effects

As can be seen in Figure 3.5, even after including compressibility and parasitic drag, there is still a discrepancy at higher AoA between the calculated and the wind tunnel data which can be attributed to flow separation. To account for these effects, correction functions (of AOA and Mach) were utilized. These functions were added manually to the drag results from SURFACES©. Similarly, the lift coefficients were adjusted for compressibility to the wind tunnel data at Mach 0.80 and 0.84.

3.5 Panel Sensitivity

A panel density study was performed to optimize the mesh size of the winglet for this thesis. The starting point was an average span-wise panel size of 1.132 in., based on the tip panel mesh. The number of panels was then varied until the error in the total aircraft drag and lift was minimized. It was found that the 1.132 in. panels already gave good results. A sample of the mesh sensitivity study is presented in Figure 3.7.

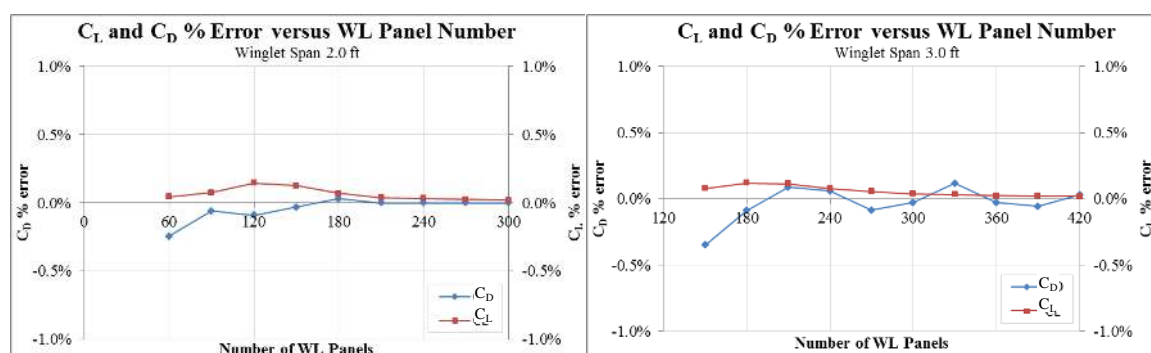


Figure 3.7. Selected Panel Sensitivity Results. The graphs show the percentage change of lift and drag coefficients with number of panels with respect to the previous mesh. The error between the different meshes is less than 0.2% for all cases.

3.6 Range Analysis

The effectiveness of the various winglets was assessed by the change in range with respect to the baseline aircraft. The range was calculated by numerical integration of the climb and cruise segments as described in the following subsections.

3.6.1 Wing Root Bending Moments

An important part of winglet analysis is the evaluation of the increase in wing root bending moment due to the additional forces at the wingtip. In this study this was assessed at the design maneuvering point of the V-n diagram at a load factor of 3 g and 220 KCAS. Under these conditions SURFACES© was used to calculate the AOA, associated loads, and root bending moment.

3.6.2 Winglet Weight

The winglet weight was estimated using Nicolai's empirical wing weight estimation equation (Nicolai & Carichner, 2010) with the calculated winglet loads:

$$W_{WL} = 0.00428(S_{WL})^{0.48} \frac{AR_{WL}(M_0)^{0.43} (L_{WL}n_z)^{0.84} (\lambda)^{0.14}}{\left(100 \frac{t}{c}\right)^{0.76} (\cos(\Lambda_{c/2}))^{1.54}} \quad (3.9)$$

Where:

S_{WL} : Winglet Area [ft²]

AR_{WL} : Winglet Aspect Ratio

M_0 : Maximum Mach number at Sea Level

L_{WL} : Lift Force on Winglets [lb_f]

n_z : Ultimate Load Factor

λ : Winglet Taper Ratio

$\Lambda_{c/2}$: Winglet Half-Chord Sweep [°]

The results were then calibrated with respect to published total winglet installation weights for the Hawker 800 business jet (Aviation Partners Inc., 2013). The Hawker 800 is slightly larger than the Falcon 10, but has a similar wing geometry and performance. In addition, no weight information for winglets on smaller business jets is publicly available, either due to the fact that no winglets have been developed for the limited number of Falcon 10 competitors, e.g. the Aérospatiale SN.601 Corvette or because the winglet has been incorporated into a design from the start and no publicly numbers are released, e.g. the Cessna 525 Citation M2.

3.6.3 Climb Segment

For the climb performance, the equations of equilibrium were solved at five second time intervals with the lift and drag coefficient values from SURFACES© and the thrust and thrust-specific fuel consumption (TSFC) from correlations following Nicolai (data summarized in Figure 3.8) (Nicolai & Carichner, 2010). A step-by-step explanation of the process is presented in Appendix A.

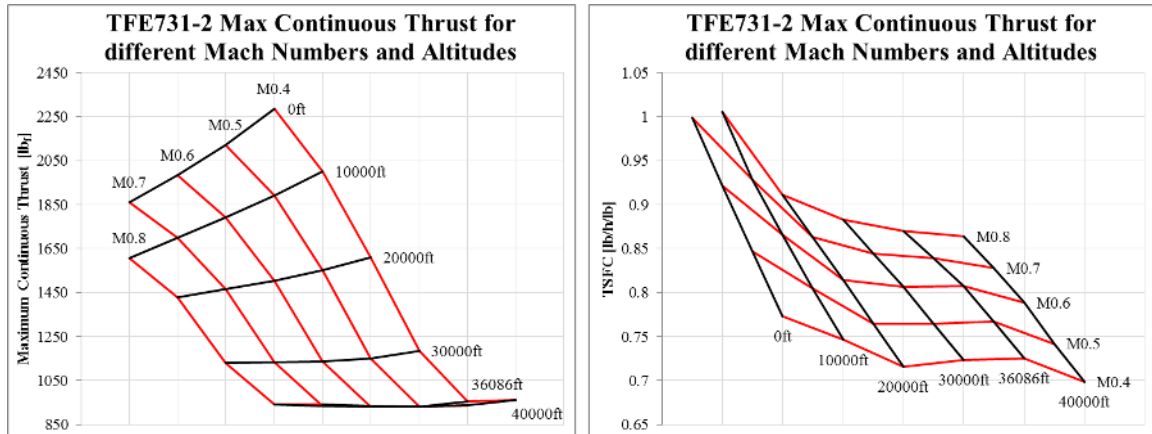


Figure 3.8. TFE731-2 Maximum Continuous Thrust and TSFC vs Altitude and Mach Number. Based on Nicolai and corrected for TFE731-2 engine variant. Note that the maximum continuous thrust at 36,089 ft. and 40,000 ft. are approximately the same.

3.6.4 Cruise Segment

The numerical range analysis was performed at a cruise altitude of 35,000 ft., starting with the top-of-climb weight W_{TOC} , calculated in previous section. The weight at the end of the cruise segment, the weight at top-of-descent W_{TOD} , was assumed to be the landing weight plus 45 min. fuel reserves plus the fuel weight from the descent obtained from Falcon 10 Operations Instruction Manual (Dassault Aviation, 1974). It was also assumed that the descent performance was not modified by the winglets, as the aircraft would operate at lower lift coefficients and therefore the winglets would have limited to no effect on the performance.

The process for the calculation of the cruise range was then similar to the climb performance analysis. The TSFC vs thrust in Figure 3.9 was employed. A detailed step-by-step explanation of the entire cruise analysis is presented in Appendix B.

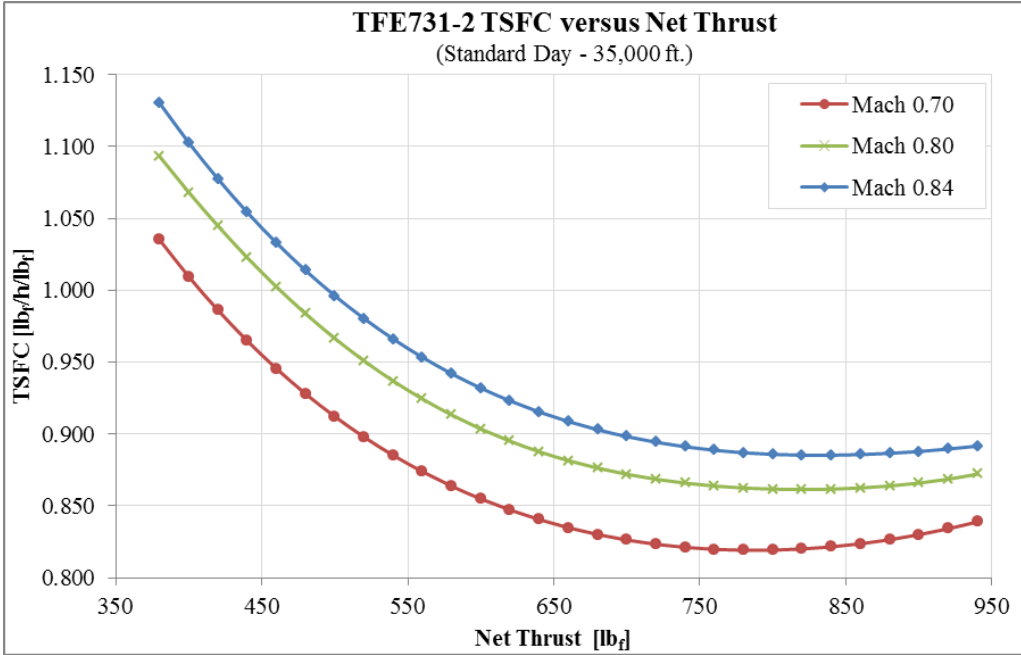


Figure 3.9. TFE731-2 TSFC vs Thrust. Graph is based on data obtained from Nicolai and corrected to represent the TFE731-2 engine variant at 35,000 ft. (Nicolai & Carichner, 2010).

3.6.5 Fuel Consumption and Savings

From the above analysis the fuel saved in cruise was calculated by comparison of the baseline and the winglet aircraft weights at the end of cruise.

Chapter IV

Results and Discussion

4.1 Effect of Winglet Configurations on Total Aircraft Drag

The following results present the change in drag with respect to the baseline aircraft for a cruise Mach number of 0.7.

Figure 4.1 shows the change in drag coefficient for four winglet configurations; two that are the best performing winglet shapes (solid lines), and two that are the least performing ones (dotted lines). The lift coefficient above which the decrease in induced drag outweighs the increase in parasitic drag is called the break-even point. The Falcon 10 cruise lift coefficient ranges from approximately 0.17 at minimum flight weight to 0.41 at W_{TOC} . Even the least efficient winglet configuration has a break-even lift coefficient of about 0.19. The Falcon 10 lift coefficient rarely drops below 0.19, even for very low weights. This leads to the conclusion that winglets will almost always improve the drag polar of the Falcon 10.

In Figure 4.1 the b2Γ90Λ225λ5 winglet has the lowest break-even point with a lift coefficient of approximately 0.129. The next winglet is the b4Γ90Λ225λ5 configuration at a break-even point of about 0.137. On the other end of the scale are the b2Γ5Λ45λ25 and b4Γ5Λ45λ25 winglets with break-even points of circa 0.175 and 0.192 respectively. It should be noted that while the shorter winglet in both cases reaches the break-even point first, due to lower parasitic drag, the larger winglet has the potential for producing greater total drag reduction.

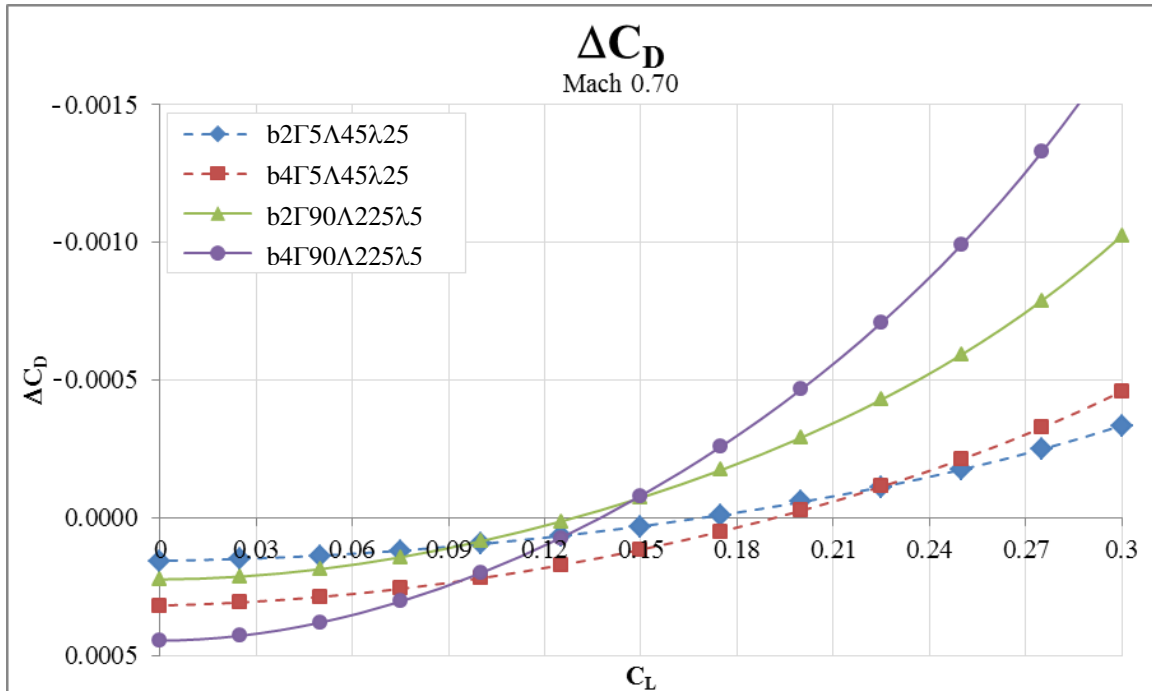


Figure 4.1. Change in Drag Coefficient with Focus on Break-Even Point. The graph shows the two best and the two worst performing configurations for their winglet span. Solid lines represent the best winglets, noted by the early crossing of the break-even point and steep rise in terms of drag reduction. The dotted lines are the least efficient winglets for higher lift coefficients. (See Figure 3.2 for explanation of winglet geometry)

The data shows that the improvements in drag are acceptable and all configurations demonstrate break-even lift coefficient points that are below the usual climb and cruise values for the Falcon 10. The worst break-even point, as noted in Figure 4.1 occurs at a lift coefficient of about 0.19, while the Falcon 10 usually has a cruise and climb lift coefficient of about 0.20 or higher. Only at very light loads, high air density, and high airspeeds does the lift coefficient go below the break-even point for some winglet configurations. In those cases it can be expected that the winglets provide less improvement over the baseline aircraft. The reduction in drag translates into aircraft L/D improvements as seen in Figure 4.2.

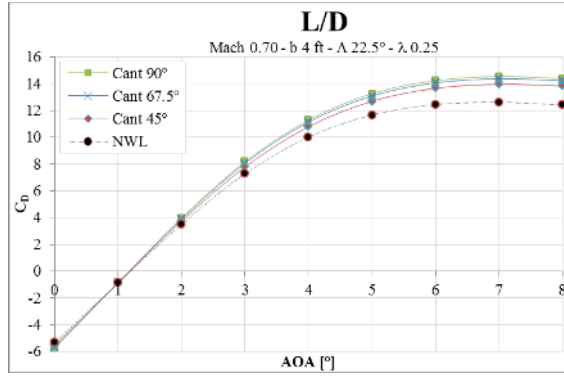


Figure 4.2. Improvement in Lift-to-Drag Ratio. The results given are for a specific geometry at different cant angles.

4.2 Winglet Weight

The estimated weight penalty due to the winglet installation is presented in Figure 4.3. If the MTOW is not modified, this increase in aircraft empty weight would result in a reduction of the aircraft payload.

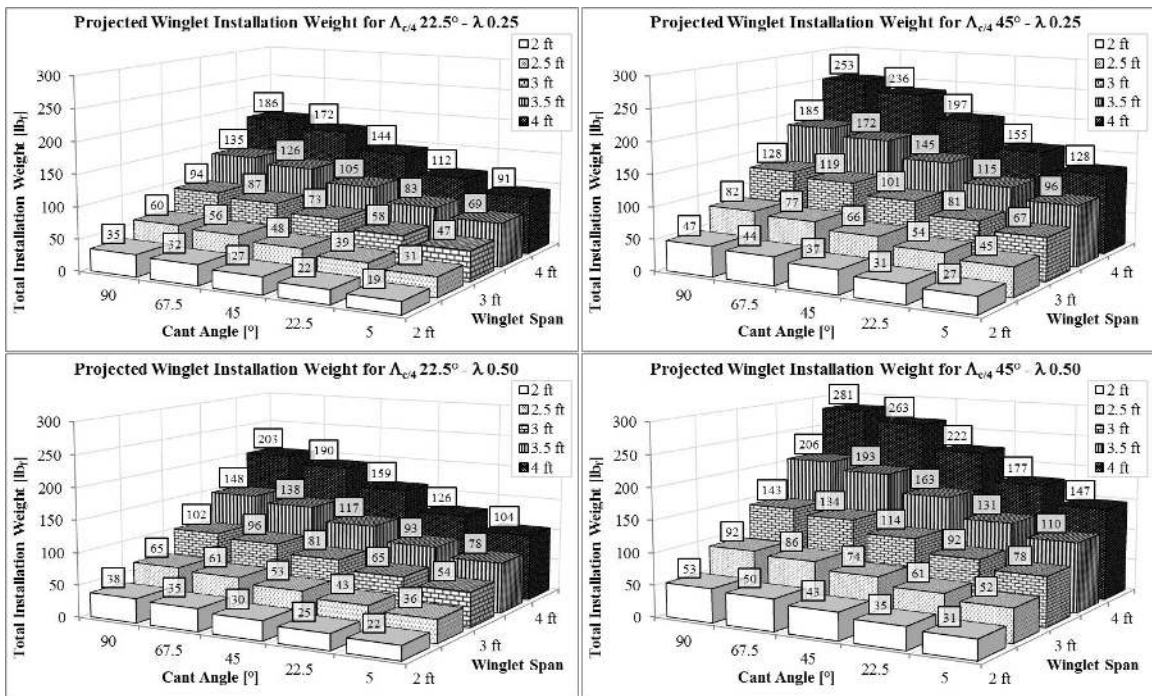


Figure 4.3. Projected Winglet Installation Weights. The weight was calculated using an empirical formula for wing weights, calibrated to a known winglet weight.

The weight estimation of the winglets is challenging due to the lack of a more specific structural model. The method followed in this thesis constitutes a reasonable attempt for a preliminary estimation. However, even small changes in the parameters have shown to vary the final weight estimate by a large factor. Therefore, the results should be used with caution until a more detailed calculation is performed.

4.3 Wing Root Bending Moment Analysis

Utilizing the built-in moment analysis tool from SURFACES© the root bending moments were found for both the baseline aircraft and the aircraft with winglets for every configuration. Included in the analysis is the bending moment relief due to the winglet weight. For the moment arm length it was assumed that the weight centroid location was at the winglet half-span. The results were then expressed in terms of a percent increase over the baseline aircraft's bending moment and are presented in Figure 4.4. Each graph depicts certain taper ratio and sweep configurations, while columns inside the graph represent the combinations of cant angle and winglet span.

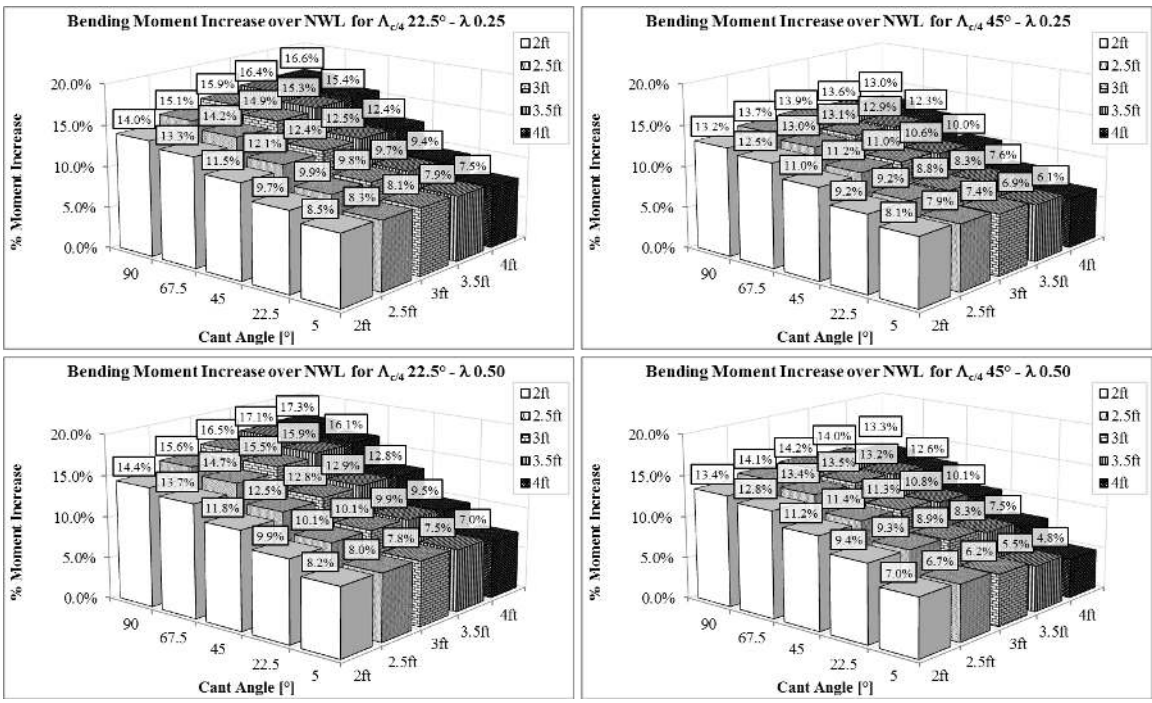


Figure 4.4. Root Bending Moment Ratio between Winglet and Baseline Aircraft. Shorter winglet span as well as lower cant angles result in lower bending moment increases compared to the baseline aircraft.

The results in Figure 4.4 show that the wing root bending moment is inversely proportional to the cant angle and directly proportional to the winglet span. However, the span effect is reduced at lower cant angles.

On the other hand, from 5° to about 45° of cant angle a steep rise in moments occurs. The largest moments are generated at 90° cant angles where the increase in moment compared to the baseline aircraft can be as large as 17 %. However, without knowledge of the Falcon 10 structural margins, no qualified statement regarding the impact of these values can be issued.

4.4 Range Analysis

The overall effect of the winglets on the aircraft is evaluated through the change in range with respect to the baseline model. Figure 4.5 through Figure 4.7 show the increases in range for the different configurations at the three Mach numbers investigated. Generally, higher cant angles result in larger range gains, even with the higher weight penalty. However, the weight penalty shows up prominently with increasing winglet spans. Furthermore, larger sweep angles as well as higher taper ratios require heavier structures, limiting the range increases.

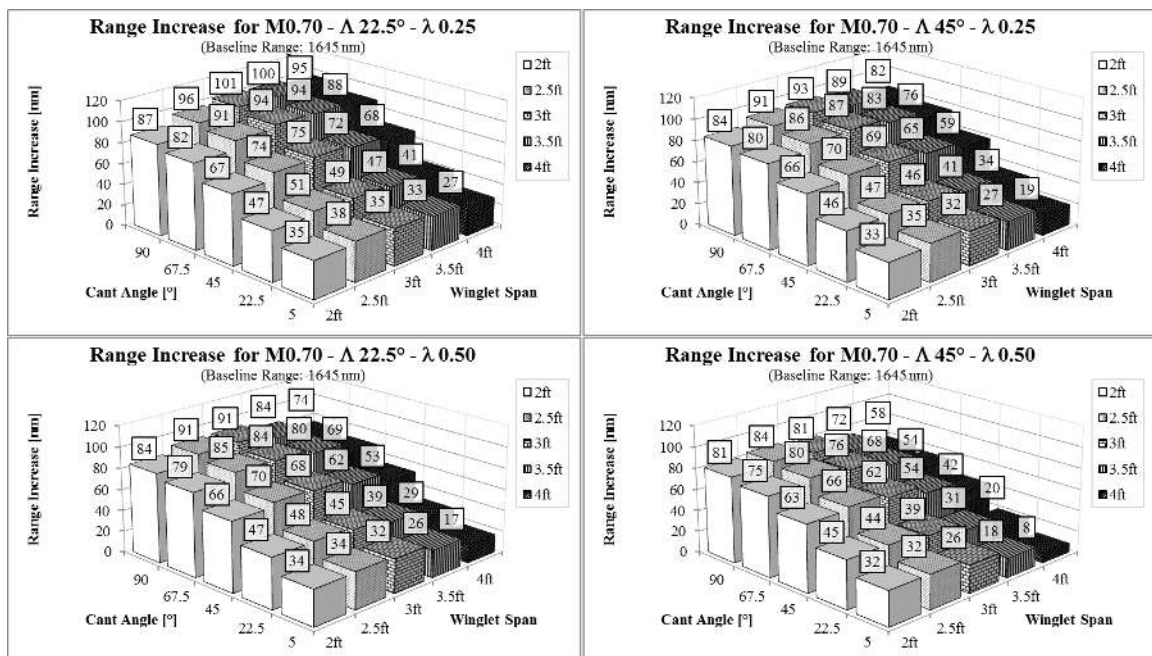


Figure 4.5. Range Increase over Baseline Aircraft for Mach 0.70 Cruise Speed.

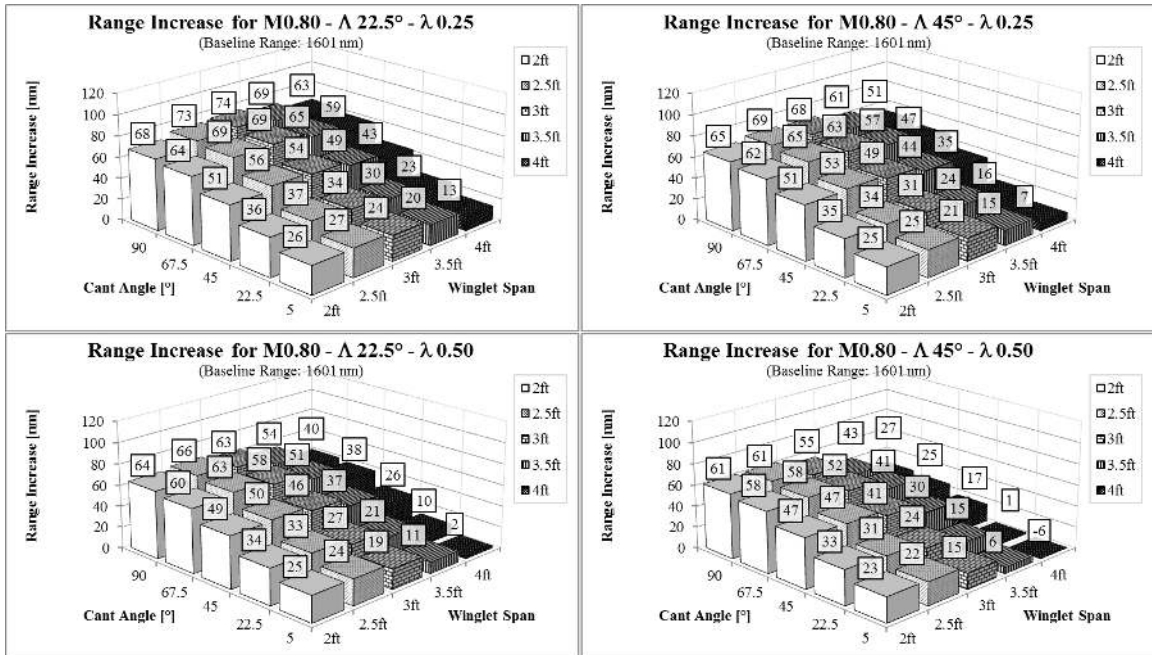


Figure 4.6. Range Increase over Baseline Aircraft for Mach 0.80 Cruise Speed.

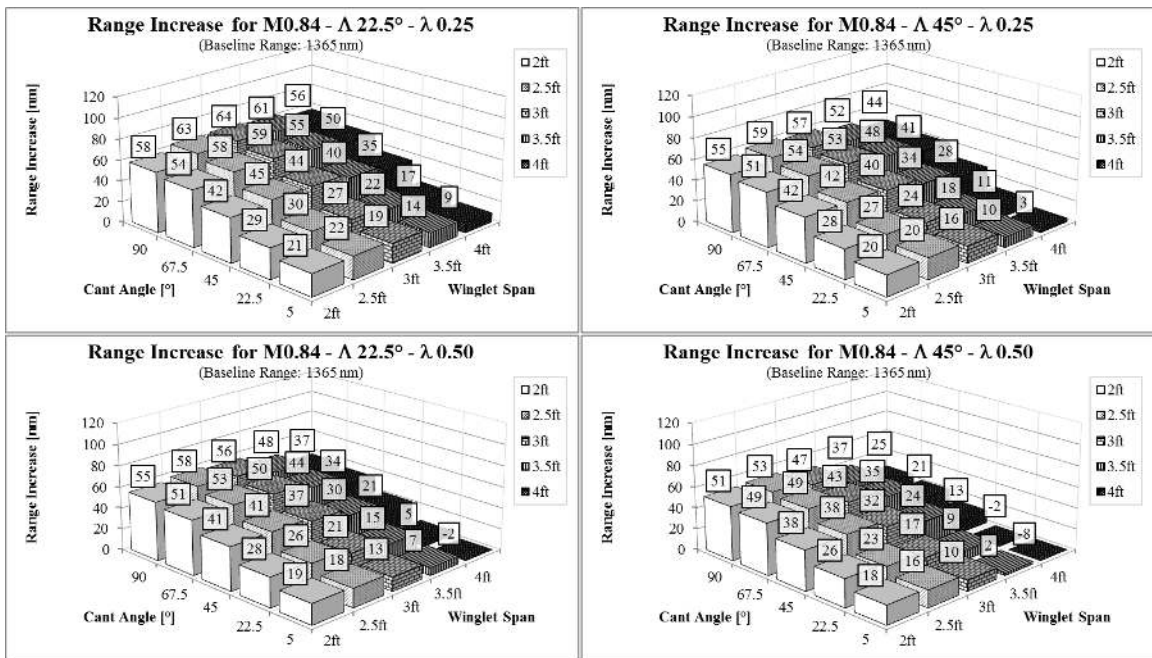


Figure 4.7. Range Increase over Baseline Aircraft for Mach 0.84 Cruise Speed.

Figure 4.5, Figure 4.6, and Figure 4.7 support the following observations regarding the effect on the range of the different geometric features of the winglet, taking into account the lost fuel capacity due to the installation weight:

1. Sweep Angle: The range increase varies from 2 to 18 nm between the 22.5° and 45° sweep angles, with lower differences for small winglet spans. Preliminarily, the sweep angle has limited effect on the winglet performance; however, while the sweep angle has been accounted for in the form factor equation (3.2), the exclusion of shock formation in VLM can skew the actual contribution of this parameter.
2. Taper Ratio: The differences between taper ratios 0.25 and 0.50 vary from 2 to 24 nm. Similar to sweep angle, the smaller the winglet span, the lower the differences between the taper ratios. Generally, the high taper ratio winglets are heavier and negate the slight lift advantage they have over the lower taper ratio wing.
3. Cant Angle: Increasing the cant angle has a noticeable effect on improving range, especially at lower values, while at higher cant angles the differences become smaller. The cant further affects the contribution of other geometric features on performance; for example, at low cant angles the differences between sweep angles or taper ratio are smaller than at higher cant angles.
4. Winglet Span: Increasing the span requires a heavier structure. For this reason, larger span winglets, despite their greater aerodynamic benefits, have smaller improvements in range than the shorter, lighter winglets.

4.5 Fuel Savings

The assessment of the fuel savings follows the same trend as the range results. However, due to the different maximum NWL ranges, the Mach 0.84 case shows a slightly higher relative fuel saving potential. Table 4.1 lists the fuel saved per nautical mile for the long range mission at MTOW for each individual configuration with the largest value of 0.0255 gal/nm for b3Γ90Λ225λ25 at Mach 0.84.

To exemplify how much could be saved in terms of fuel cost a fuel price of \$5.47/gal (current for May 1st, 2014) was used and the results are presented in Table 4.2.

The results for the cost reduction due to winglets are based on the current fuel price, which varies greatly not only in time but also with location. For example, from the AirNav source, the lowest fuel price at the time sampled (May 1st, 2014) was \$3.89 and the highest \$9.51, with an average fuel price of \$5.47.

If winglet configuration b25Γ675Λ225λ25 would be installed, an operator would save 0.0217 gal/nm at Mach 0.70 when flying the original NWL maximum range of 1,645 nm. Table 4.3 presents how the different fuel prices would turn out for this winglet in terms of potential yearly cost savings for 50 flights per year at the NWL maximum range profile.

Table 4.1

Fuel Saved per Nautical Mile. The decrease in drag due to winglets means that less thrust has to be produced, leading to a slight reduction in fuel burn. The table lists the fuel saved in US-Gallons for each nautical mile flown.

Span ? Cant [°]	Fuel saved [gal/nm] - Config.: TR0.25 - Sw 45°					Fuel saved [gal/nm] - Config.: TR0.50 - Sw 22.5°					Fuel saved [gal/nm] - Config.: TR0.50 - Sw 45°					
	2ft	2.5ft	3ft	3.5ft	4ft	2ft	2.5ft	3ft	3.5ft	4ft	2ft	2.5ft	3ft	3.5ft	4ft	
Mach 0.70	90	0.0219	0.0242	0.0252	0.0251	0.0242	0.0212	0.0228	0.0229	0.0216	0.0193	0.0212	0.0231	0.0236	0.0228	0.0213
	67.5	0.0207	0.0229	0.0238	0.0236	0.0227	0.0200	0.0217	0.0216	0.0205	0.0182	0.0202	0.0219	0.0222	0.0215	0.0199
	45	0.0170	0.0186	0.0190	0.0186	0.0178	0.0166	0.0177	0.0175	0.0162	0.0143	0.0166	0.0180	0.0179	0.0169	0.0156
Mach 0.80	90	0.0188	0.0205	0.0208	0.0200	0.0184	0.0183	0.0195	0.0193	0.0179	0.0157	0.0179	0.0188	0.0181	0.0160	0.0129
	67.5	0.0178	0.0193	0.0195	0.0188	0.0172	0.0174	0.0185	0.0182	0.0169	0.0146	0.0169	0.0178	0.0169	0.0152	0.0121
	45	0.0146	0.0156	0.0154	0.0144	0.0130	0.0143	0.0151	0.0144	0.0129	0.0110	0.0138	0.0144	0.0134	0.0114	0.0089
Mach 0.84	90	0.0226	0.0246	0.0252	0.0245	0.0229	0.0218	0.0233	0.0231	0.0215	0.0191	0.0216	0.0228	0.0222	0.0201	0.0168
	67.5	0.0211	0.0230	0.0233	0.0226	0.0209	0.0205	0.0218	0.0214	0.0200	0.0175	0.0201	0.0213	0.0204	0.0186	0.0152
	45	0.0168	0.0180	0.0178	0.0166	0.0150	0.0164	0.0173	0.0165	0.0147	0.0125	0.0160	0.0166	0.0155	0.0132	0.0103
Mach 0.90	90	0.0115	0.0118	0.0110	0.0096	0.0076	0.0112	0.0111	0.0101	0.0083	0.0058	0.0110	0.0107	0.0092	0.0069	0.0037
	67.5	0.0082	0.0087	0.0077	0.0062	0.0042	0.0079	0.0080	0.0066	0.0046	0.0023	0.0075	0.0074	0.0058	0.0036	0.0007
	45	0.0073	0.0078	0.0066	0.0050	0.0030	0.0073	0.0074	0.0063	0.0047	0.0028	0.0067	0.0062	0.0046	0.0023	-0.0006

Table 4.2

US-Dollar Savings per Nautical Mile. Using a fuel price of \$5.47 per gallon of Jet-A fuel (see Note), the numbers present the amount of US-Dollars saved for each nm flown. Multiplying the value by distance would give the total amount of money saved on that trip distance.

Span ? Cant [°]	Saving for 1 nm - Config.: TR0.25 - Sw22.5°					Saving for 1 nm - Config.: TR0.25 - Sw45°					Saving for 1 nm - Config.: TR0.50 - Sw22.5°					Saving for 1 nm - Config.: TR0.50 - Sw45°										
	2ft	2.5ft	3ft	3.5ft	4ft	2ft	2.5ft	3ft	3.5ft	4ft	2ft	2.5ft	3ft	3.5ft	4ft	2ft	2.5ft	3ft	3.5ft	4ft	2ft	2.5ft	3ft	3.5ft	4ft	
90	\$ 0.12	\$ 0.13	\$ 0.14	\$ 0.14	\$ 0.13	\$ 0.12	\$ 0.12	\$ 0.13	\$ 0.12	\$ 0.11	\$ 0.12	\$ 0.13	\$ 0.12	\$ 0.12	\$ 0.12	\$ 0.11	\$ 0.12	\$ 0.13	\$ 0.12	\$ 0.12	\$ 0.12	\$ 0.11	\$ 0.12	\$ 0.11	\$ 0.10	\$ 0.09
67.5	\$ 0.11	\$ 0.13	\$ 0.13	\$ 0.13	\$ 0.12	\$ 0.11	\$ 0.12	\$ 0.12	\$ 0.11	\$ 0.10	\$ 0.11	\$ 0.12	\$ 0.12	\$ 0.12	\$ 0.11	\$ 0.10	\$ 0.11	\$ 0.12	\$ 0.12	\$ 0.12	\$ 0.11	\$ 0.11	\$ 0.11	\$ 0.11	\$ 0.10	\$ 0.08
45	\$ 0.09	\$ 0.10	\$ 0.10	\$ 0.10	\$ 0.10	\$ 0.09	\$ 0.10	\$ 0.10	\$ 0.09	\$ 0.08	\$ 0.09	\$ 0.10	\$ 0.09	\$ 0.09	\$ 0.08	\$ 0.07	\$ 0.08	\$ 0.09	\$ 0.09	\$ 0.09	\$ 0.09	\$ 0.09	\$ 0.09	\$ 0.09	\$ 0.08	\$ 0.06
22.5	\$ 0.07	\$ 0.07	\$ 0.07	\$ 0.07	\$ 0.06	\$ 0.06	\$ 0.07	\$ 0.06	\$ 0.06	\$ 0.04	\$ 0.06	\$ 0.07	\$ 0.06	\$ 0.06	\$ 0.05	\$ 0.04	\$ 0.05	\$ 0.06	\$ 0.06	\$ 0.05	\$ 0.05	\$ 0.06	\$ 0.06	\$ 0.06	\$ 0.05	\$ 0.03
5	\$ 0.05	\$ 0.05	\$ 0.05	\$ 0.05	\$ 0.04	\$ 0.05	\$ 0.05	\$ 0.05	\$ 0.04	\$ 0.03	\$ 0.05	\$ 0.05	\$ 0.05	\$ 0.04	\$ 0.03	\$ 0.04	\$ 0.05	\$ 0.05	\$ 0.05	\$ 0.04	\$ 0.03	\$ 0.05	\$ 0.05	\$ 0.04	\$ 0.03	\$ 0.01
90	\$ 0.10	\$ 0.11	\$ 0.11	\$ 0.11	\$ 0.10	\$ 0.10	\$ 0.11	\$ 0.11	\$ 0.10	\$ 0.09	\$ 0.10	\$ 0.10	\$ 0.10	\$ 0.09	\$ 0.07	\$ 0.09	\$ 0.09	\$ 0.10	\$ 0.09	\$ 0.07	\$ 0.07	\$ 0.09	\$ 0.09	\$ 0.10	\$ 0.07	\$ 0.05
67.5	\$ 0.10	\$ 0.11	\$ 0.11	\$ 0.11	\$ 0.09	\$ 0.10	\$ 0.10	\$ 0.10	\$ 0.09	\$ 0.08	\$ 0.09	\$ 0.10	\$ 0.09	\$ 0.08	\$ 0.07	\$ 0.09	\$ 0.09	\$ 0.09	\$ 0.08	\$ 0.07	\$ 0.07	\$ 0.09	\$ 0.09	\$ 0.08	\$ 0.07	\$ 0.05
45	\$ 0.08	\$ 0.09	\$ 0.08	\$ 0.08	\$ 0.07	\$ 0.08	\$ 0.08	\$ 0.08	\$ 0.07	\$ 0.06	\$ 0.08	\$ 0.08	\$ 0.07	\$ 0.06	\$ 0.05	\$ 0.07	\$ 0.07	\$ 0.07	\$ 0.06	\$ 0.05	\$ 0.05	\$ 0.07	\$ 0.07	\$ 0.07	\$ 0.05	\$ 0.03
22.5	\$ 0.06	\$ 0.06	\$ 0.05	\$ 0.05	\$ 0.04	\$ 0.06	\$ 0.06	\$ 0.06	\$ 0.04	\$ 0.03	\$ 0.06	\$ 0.06	\$ 0.05	\$ 0.04	\$ 0.02	\$ 0.05	\$ 0.05	\$ 0.05	\$ 0.04	\$ 0.02	\$ 0.02	\$ 0.05	\$ 0.05	\$ 0.04	\$ 0.03	\$ 0.01
5	\$ 0.04	\$ 0.04	\$ 0.04	\$ 0.03	\$ 0.02	\$ 0.04	\$ 0.04	\$ 0.04	\$ 0.03	\$ 0.02	\$ 0.04	\$ 0.04	\$ 0.03	\$ 0.03	\$ 0.02	\$ 0.03	\$ 0.04	\$ 0.04	\$ 0.03	\$ 0.02	\$ 0.01	\$ 0.04	\$ 0.03	\$ 0.03	\$ 0.01	\$ -0.00
90	\$ 0.12	\$ 0.13	\$ 0.14	\$ 0.13	\$ 0.13	\$ 0.12	\$ 0.13	\$ 0.13	\$ 0.12	\$ 0.10	\$ 0.12	\$ 0.13	\$ 0.12	\$ 0.11	\$ 0.09	\$ 0.11	\$ 0.12	\$ 0.12	\$ 0.11	\$ 0.09	\$ 0.09	\$ 0.11	\$ 0.11	\$ 0.11	\$ 0.09	\$ 0.07
67.5	\$ 0.12	\$ 0.13	\$ 0.13	\$ 0.13	\$ 0.11	\$ 0.11	\$ 0.12	\$ 0.12	\$ 0.11	\$ 0.10	\$ 0.11	\$ 0.12	\$ 0.11	\$ 0.10	\$ 0.08	\$ 0.11	\$ 0.12	\$ 0.11	\$ 0.10	\$ 0.08	\$ 0.08	\$ 0.11	\$ 0.11	\$ 0.10	\$ 0.10	\$ 0.06
45	\$ 0.09	\$ 0.10	\$ 0.10	\$ 0.09	\$ 0.08	\$ 0.09	\$ 0.09	\$ 0.09	\$ 0.08	\$ 0.07	\$ 0.09	\$ 0.09	\$ 0.08	\$ 0.07	\$ 0.06	\$ 0.08	\$ 0.08	\$ 0.08	\$ 0.07	\$ 0.06	\$ 0.06	\$ 0.08	\$ 0.08	\$ 0.07	\$ 0.06	\$ 0.04
22.5	\$ 0.06	\$ 0.06	\$ 0.06	\$ 0.05	\$ 0.04	\$ 0.06	\$ 0.06	\$ 0.06	\$ 0.05	\$ 0.03	\$ 0.06	\$ 0.06	\$ 0.05	\$ 0.04	\$ 0.02	\$ 0.06	\$ 0.06	\$ 0.05	\$ 0.04	\$ 0.02	\$ 0.02	\$ 0.06	\$ 0.05	\$ 0.04	\$ 0.03	\$ 0.01
5	\$ 0.04	\$ 0.05	\$ 0.04	\$ 0.03	\$ 0.02	\$ 0.04	\$ 0.04	\$ 0.04	\$ 0.03	\$ 0.01	\$ 0.04	\$ 0.04	\$ 0.03	\$ 0.02	\$ 0.00	\$ 0.04	\$ 0.04	\$ 0.03	\$ 0.02	\$ 0.00	\$ 0.04	\$ 0.04	\$ 0.03	\$ 0.01	\$ 0.01	\$ -0.01

Note: Fuel savings are based on an average US-nationwide fuel price of \$5.47 per gallon of Jet-A fuel as reported by www.airnav.com May 1st, 2014 (AirNav, LLC, 2014).

Table 4.3

Cost savings for b25T675A225λ25. Annual savings variation with different fuel prices for the specified winglet configuration if operated at the maximum range mission for 50 flights per year.

Price range	Low	Average	High	
Fuel Saved		0.0217		gal/nm
Fuel Price	\$3.89	\$5.47	\$9.51	\$/gal
Fuel Saved	\$0.08	\$0.12	\$0.21	\$/nm
Mission Range		1645		nm
Savings/flight	\$138.86	\$195.26	\$339.47	\$/flight
Flights/year		50		flights/y
Savings/year	\$6,942.97	\$9,762.99	\$16,973.69	\$/y

Chapter V

Conclusion and Recommendations

5.1 General Observations

The preliminary study of the feasibility of installation of winglets on the Falcon 10 wing shows that the drag is reduced at the usual cruise lift coefficient ranges.

In terms of range, the improvements over the baseline aircraft were rather limited for some configurations.

The general characteristics of the different winglet configurations were in line with the expectations set by previous research and assumptions. The limited effect of taper ratio and sweep on the performance was one of the smaller, but notable discoveries during the data analysis; however, it is possible that the limitations of the analysis, inherent to VLM codes, like neglecting shock interactions, obscure other positive or negative effects of those parameters.

5.2 Conclusion

The preliminary study shows that adding winglets to the Dassault Falcon 10 business jet can offer economic benefits. Range was one of the primary concerns for customers, with possible fuel savings a close secondary request. However, none of these parameters can be looked at on an isolated basis and the effect on wing root bending moments and associated weight increase should be carefully studied to conclude that a certain winglet is viable option for retrofit. Additionally, any retrofit will be subject to a supplemental type certificate (STC), which governs the installation of any new

component on a certified aircraft. Advisory Circular AC 21-40A provides an outline of the STC application process and states that:

A type design change is classified as minor or major (see 14 CFR § 21.93). A minor change has no appreciable effect on the weight, balance, structural strength, reliability, operational characteristics, or other characteristics affecting the airworthiness of the product. [...] All other changes are major changes. In addition to being classified as minor or major change, and to comply with 14 CFR part 36, a type design change may be classified as an acoustical change. (FAA, 2007)

It further states that all changes must comply with applicable regulations and airworthiness standards and demonstration of compliance has to be performed by ground and flight tests.

Another certification issue is the ICAO and FAA airport classification of aircraft. Increasing the wingspan can potentially place the aircraft into a new category which could limit the number of airports the aircraft can operate in and out of. For the Falcon 10 the wingspan has to maintain 49 ft. or lower to stay in its original FAA Class B-I. This means that of the tested winglets those with cant angles $\geq 67.5^\circ$ as well as winglet spans ≥ 3.5 ft. would require a change in classification.

Finally, the project demonstrates that VLM is a good preliminary tool to narrow down the winglet configurations to a few winglets that could be candidates for higher fidelity evaluations.

5.2.1 *Recommended Winglet Shape for Detailed Research*

The results recommend a winglet with low taper ratio and high cant angle, even at the cost of higher bending moments. This is offset partially by using a shorter winglet span with lower weight penalty as well as a smaller moment increase. The fact that Dassault, as well as other sources, state that the Falcon 10 is exceptionally well engineered and features “a rugged build quality usually reserved for fighter jets” (Huber, 2012) would suggest that the structure has some built-in margins that would be able to cope with the increased wing root bending moments without significant wing modifications.

To find possible optimum winglet configurations for further research, the results were evaluated by setting a variety of boundary conditions in terms of range, moment, and saving increases. The range increase should be more than 90 nm with a moment increase no more than 15%, while having a fuel saving of more than 0.0222 gal/nm.

Based on these restrictions, the most promising winglet configuration would be b3Γ90Λ45λ25, which would represent a raked wingtip configuration similar to Figure 2.2d. This raked wingtip would save 37.67 gal of fuel if flying according to the original maximum NWL mission of 1,645 nm at Mach 0.70, or would increase that range by 93 nm to 1,738 nm. The root bending moment is estimated to be 13.9% higher than the baseline aircraft; however, this has to be examined in more detailed structural analyses. If bending moments are of concern, reducing the cant angle up to 45° would still provide potential benefits that might be valid for further design iterations.

With best configurations established Figure 5.1a presents the most promising final product and Figure 5.1b an alternative, reduced cant configuration.



Figure 5.1. Dassault Falcon 10RX and 10LX. This edit shows how the Falcon 10 could appear if a) the recommended raked wingtips b) reduced cant raked winglets would be installed (Pictures by author).

5.3 Recommendations for Future Research

Being this a preliminary study of winglets, further research will have to be performed in terms of detailed aerodynamic and structural properties.

VLM codes display limitations with regards to high AOA or flow interference at the junction between wing and the winglet. It is recommended to study the possible winglets with Navier-Stokes solvers or in actual wind tunnel tests. Further aerodynamic characteristics that need to be looked into are possible shockwave formation and interactions.

Aircraft stability is an additional area that needs to be investigated to ensure that no considerable degradation of the flight characteristics occurs, especially as canted winglets can have a pronounced dihedral effect.

A simplified winglet weight estimation method would be of great value. Also a detailed structural analysis of a possible winglet and its supporting structure has to be conducted to ensure integrity and consequently to obtain precise weight values. The “structural problems encountered in retrofitting a tip modification to an existing wing can only be determined by a detailed analysis of the existing structure” (Heyson, Riebe, & Fulton, 1977). Once the structural details are established, it will be possible to investigate the potential effect of varying the toe-out angle and airfoil, which allows loading up the winglets more and increase range further than currently predicted.

It is recommended focusing further research efforts on winglets with cant angles of 45° or larger, small taper ratios of 0.25 ± 0.05 as well as sweep angles in the range of 30° to 45° . Winglet span should be kept around 2.5 ± 0.5 ft., depending on cant angle and more precise weight estimations.

References

- AirNav, LLC. (2014, March 11). *Fuel Price Report*. Retrieved March 11, 2014, from AirNav: <https://www.airnav.com/fuel/report.html>
- Aviation Partners Inc. (2013, March 22). *Blended Winglets For The Hawker 800 And Hawker 800XP*. Retrieved April 14, 2014, from Aviation Partners Inc.: <http://www.aviationpartners.com/hawker.html>
- Barber, M. R., Selegan, D., Montoya, L., Jacobs, P., Flechner, S., Sims, R., . . . W., M. (1981). KC-135 Winglet Program Review. *Symposium Dryden Flight Research Center*. Edwards: NASA Ames Research Center - Dryden Flight Research Facility.
- Dassault Aviation. (1974, February 20). Falcon 10 Operational Instructional Manual. *Revision 12*.
- Dassault Aviation. (2013). *Mystère-Falcon 10-100*. Retrieved March 22, 2014, from Dassault Aviation Web site: <http://www.dassault-aviation.com/en/passion/aircraft/civil-dassault-aircraft/mystere-falcon-10-100/>
- FAA. (2007). *Guide For Obtaining A Supplemental Type Certificate*. FAA, Aircraft Engineering Division. Washington: FAA.
- Faye, R., Laprete, R., & Winter, M. (2002). Blended Winglets for Improved Aircraft Performance. *AERO*(17), 16-31.
- Gudmundsson, S. (2014). *General Aviation Aircraft Design: Applied Methods and Procedures* (1st ed.). New York: Butterworth-Heinemann.
- Great OWL. (2009, August). *SURFACES User Manual*. Great OWL Publishing.

- Heyson, H. H., Riebe, G. D., & Fulton, C. L. (1977). *Theoretical Parametric Study of the Relative Advantages of Winglets and Wing-Tip Extensions*. NASA Langley Research Center, Scientific and Technical Information Office. Hampton: NASA.
- Huber, M. (2012, December 4). *Dassault Falcon 10/100*. Retrieved April 14, 2014, from Business Jet Traveler: <http://www.bjtonline.com/business-jet-news/dassault-falcon-10100>
- Lundry, J. (1968). *A Numerical Solution For The Minimum Induced Drag, And The Corresponding Loading, Of Nonplanar Wings*. Langley Research Center. Long Beach: NASA.
- McLean, D. (2005). Wingtip Devices: What They Do And How They Do It. *Performance and Flight Operations Engineering Conference*. Boeing.
- Nicolai, L. M., & Carichner, G. E. (2010). *Fundamentals Of Aircraft And Airship Design Volume I - Aircraft Design* (Vol. I). Reston, Virginia, United States of America: AIAA. Retrieved November 13, 2013
- Whitcomb, R. T. (1976). *A Design Approach And Selected Wind-Tunnel Results At High Subsonic Speeds For Wing-Tip Mounted Winglets*. Langley Research Center, NASA. Hampton: NASA.

Bibliography

- Anderson, J. D. (2011). *Fundamentals Of Aerodynamics* (5th ed.). New York: McGraw-Hill.
- Babigian, R., & Hayashibara, S. (2009). *Computational Study Of Vortex Wake Generated By A Three-Dimensional Wing With Dihedral, Taper, And Sweep*. Embry-Riddle Aeronautical University, College of Engineering. Prescott: AIAA.
- Dassault Aviation. (1973, October 17). Falcon 10 Airplane Flight Manual. *Revision 25*.
- Dassault Aviation. (1973, November 30). Falcon 10 Descriptive Manual - Book 1. *Revision 15*.
- Flechner, S. G., & Jacobs, P. F. (1976). *A High Subsonic Speed Wind-Tunnel Investigation Of Winglets On A Representative Second-Generation Jet Transport Wing*. NASA Langley Research Center. Hampton: NASA.
- Gratzer, L. B. (1993, February 1). *Patent No. 5,348,253*. United States of America. Research Center, Scientific and Technical Information Office. Hampton: NASA.
- JetAdvisors. (2012, August 16). *Winglets: To Winglet, Or Not To Winglet?* Retrieved from JetAdvisors: <http://jetadvisors.com/winglets/>
- Jones, R., & Lasinski, T. (1980). *Effect Of Winglets On The Induced Drag Of Ideal Wing Shapes*. NASA Ames Research Center. Moffet Field: NASA.
- Lacy, C. (2001). Aviation Partners Winglet Debut On Hawker 800. *Professional Pilot*, 102-105.
- Meyer Jr., R. R., & Covell, P. F. (1986). *Effects Of Winglets On A First Generation Jet Transport Wing*. NASA Ames Research Center, Dryden Flight Research Facility. Edwards: NASA.

- Montoya, L. C., Flechner, S. G., & Jacobs, P. F. (1978). *Effect Of An Alternate Winglet On The Pressure And Spanwise Load Distribution Of A First-Generation Jet Transport Wing*. NASA Langley Research Center. Hampton: NASA.
- Pester, M. (2010). *Multi-Disciplinary Conceptual Aircraft Design Using CEASIOM*. Hochschule für Angewandte Wissenschaften Hamburg, Department Fahrzeugtechnik und Flugzeugbau. Hamburg: Hamburg University of Applied Sciences.
- Priyono, E. (1994). *An Investigation Of The Transonic Pressure Drag Coefficient For Axi-Symmetric Bodies*. Monterey: Naval Postgraduate School.
- Rauch, F. J., & Waters, C. (1978). *Analyses And Initial Tests Of A 1/6.5-Size Flutter Model Of An Executive-Jet-Transport Supercritical Wing With/Without Winglet*. Grumman Aerospace Corporation. Washington: NASA.
- Raymer, D. P. (2012). *Aircraft Design: A Conceptual Approach* (5th ed.). Reston: AIAA.
- Safranek, M. J. (2008). *No Winglets: What A Drag... Argument For Adding Winglets To A Large Air Force Aircraft*. Marine Corps University, Marine Corps Combat Development Command, Command and Staff College. Quantico: United States Marine Corps.
- Shollenberger, C. (1979). *Application Of An Optimized Wing-Winglet Configuration To An Advanced Commercial Transport*. McDonnell Douglas Corporation, Douglas Aircraft Company. Long Beach: NASA.
- Soltani, M. R., Ghorbanian, K., & Nazarinia, M. (2004). *Experimental Investigation Of The Effect Of Various Winglet Shapes On The Total Pressure Distribution Behind*

A Wing. Sharif University of Technology, Department of Aerospace Engineering.
Tehran: ICAS.

Taylor, A. (1983). *DC-10 Winglet Flight Evaluation Summary Report*. NASA Langley
Research Center. Hampton: NASA.

Weierman, J., & Jacob, J. D. (2010). *Winglet Design And Optimization For UAVs*.
Oklahoma State University, School of Mechanical & Aerospace Engineering.
Stillwater: AIAA.

Yates, J. E., & Donaldson, C. d. (1986). *A Fundamental Study Of Drag And An
Assessment Of Conventional Drag-Due-To-Lift Reduction Devices*. NASA
Langley Research Center. Hampton: NASA.

Appendix A

Climb Performance Analysis Process

For the climb performance it was assumed that the aircraft would climb with a constant airspeed of 260 kt at maximum continuous thrust setting. The Falcon 10 uses the Garrett TFE731 engine for which Nicolai provides data. A small correction had to be incorporated to derive the Falcon 10's TFE731-2 variant from the TFE731-1069 engine data presented in the book (Nicolai & Carichner, 2010). The reference shows the net installed thrust vs fuel flow for SL, 10,000, 20,000, 30,000, and 36,089 ft. altitudes.

Starting at sea level the air density ρ and air density ratio σ were calculated by:

$$\rho = 0.002378 \cdot (1 - 0.0000068756h)^{4.2561} \quad (\text{A.1})$$

Where:

h : Altitude [ft.]

And

$$\sigma = (1 - 0.0000068756h)^{4.2561} \quad (\text{A.2})$$

The airspeed of 260 KCAS had to be converted to true airspeed in ft./s, and from KTAS to feet per second, utilizing the simplified conversion equation (Gudmundsson, 2014)

$$V_{TAS} = 1.688 \cdot KTAS = 1.688 \cdot \frac{KCAS}{\sqrt{\sigma}} \quad (\text{A.3})$$

Where:

KTAS: True Airspeed in Knots

KCAS: Calibrated Airspeed in Knots

Additionally, the speed also had to be expressed in Mach because the thrust and TSFC values were given in Figure 3.8 as a function of Mach number. The conversion used was:

$$M = \frac{V_{TAS}}{1116\sqrt{1-0.0000068756h}} \quad (A.4)$$

These equations established the atmospheric and speed related parameters for the climb analysis.

Next are the parameters that deal with the aircraft itself, with the weight initialized at MTOW and then progressively reduced by the fuel amount burned in the previous calculation step. Using the assumption that weight equals lift, the instantaneous lift coefficient was obtained from the standard lift equation.

That lift coefficient was used in the appropriate drag polar (particular to each winglet configuration) to calculate the drag coefficient from which the drag force was computed.

Figure 3.8 was used to find the maximum continuous thrust and TSFC at the specific altitude and then applied to a) the calculation of excess power and b) the amount of fuel burned in the time step. To find the fuel burned, the same equation used in the cruise performance, (B.1) was used. The resulting fuel burned was subtracted from the initial weight to obtain the new weight for the next iteration step.

The rate-of-climb (RoC) was calculated with (Gudmundsson, 2014):

$$V_V = \frac{T \cdot V_{TAS} - D \cdot V_{TAS}}{W} \quad (\text{A.5})$$

Where:

T : Thrust Force [lb_f]

D : Drag Force [lb_f]

W : Aircraft Weight [lb_f]

With the RoC found, the last step was to find the new altitude for the next iteration by taking the altitude from the current iteration and adding the altitude covered by:

$$h_{n+1} = h_n + V_V \cdot \Delta t \quad (\text{A.6})$$

Where:

h_n : Initial altitude at current iteration

Δt : Time step [s]

The new weight and altitude were the starting values for the next iteration and the calculations were looped until a specified level off altitude was reached, which was 35,000 ft. for the cruise analysis. The final weight upon reaching 35,000 ft. was subtracted from the take-off weight to find the amount of fuel burned during the climb segment.

The total distance the aircraft traveled in the climb was recorded by summing up the distances covered during each time step, which for the climb analysis was five

seconds. The distances covered in each iteration was simply the true airspeed multiplied by the time step.

Appendix B

Cruise Performance Analysis Process

The numerical range analysis was performed at a cruise altitude of 35,000 ft., with the starting weight being the weight at top-of-climb W_{TOC} as calculated in the climb analysis. The weight at the end of the cruise segment, the weight at top-of-descent W_{TOD} , is the landing weight plus 45 min. fuel reserves plus the fuel weight from the descent. These numbers are found from data in the Falcon 10 Operations Instruction Manual.

With the weights determined, the next steps were carried out as presented in the climb performance analysis. The lift coefficient was found using the lift equation while the drag coefficients came from the C_D vs C_L trendlines and the actual drag force was calculated by the drag equation.

To find the thrust required at the particular time step, the thrust was set equal to the drag. This value was then combined with the TSFC to find the mass outflow, which is the fuel consumed. Using Figure 3.9, trendlines were used to equate the TSFC to the specific thrust at the time step in question and then the instantaneous TSFC was entered into the equation:

$$\dot{m} = \text{TSFC} \cdot T \cdot \Delta t \quad (\text{B.1})$$

Where:

TSFC: Thrust specific fuel consumption [$\text{lb}_f/\text{s}/\text{lb}_f$]

The expended fuel weight was then subtracted to get the new aircraft weight for the next calculation iteration so that:

$$W_{n+1} = W_n - \dot{m} \quad (\text{B.2})$$

Where:

W_n : Weight at start of old time step [lb_f]

For each weight iterations performed, the distance covered was recorded by multiplying the time step (in seconds) and the ground speed (in feet per second), i.e. 680.9 ft./s for Mach 0.70, 778.2 ft./s for Mach 0.80, and 817.0 ft./s for Mach 0.84. Initially, larger time steps were chosen, but a finer resolution appeared to be necessary and 10 second increments were selected. Once the iterations reached the calculated top-of-descend weight, the individual distances were summed up to give the total range.

Appendix C

SURFACES© Validation Examples

The graphs presented in Figure C.1, Figure C.2, and Figure C.3 are validation examples taken, with permission by GreatOWL Publishing, from the SURFACES© user manual to confirm the program's computational capability.

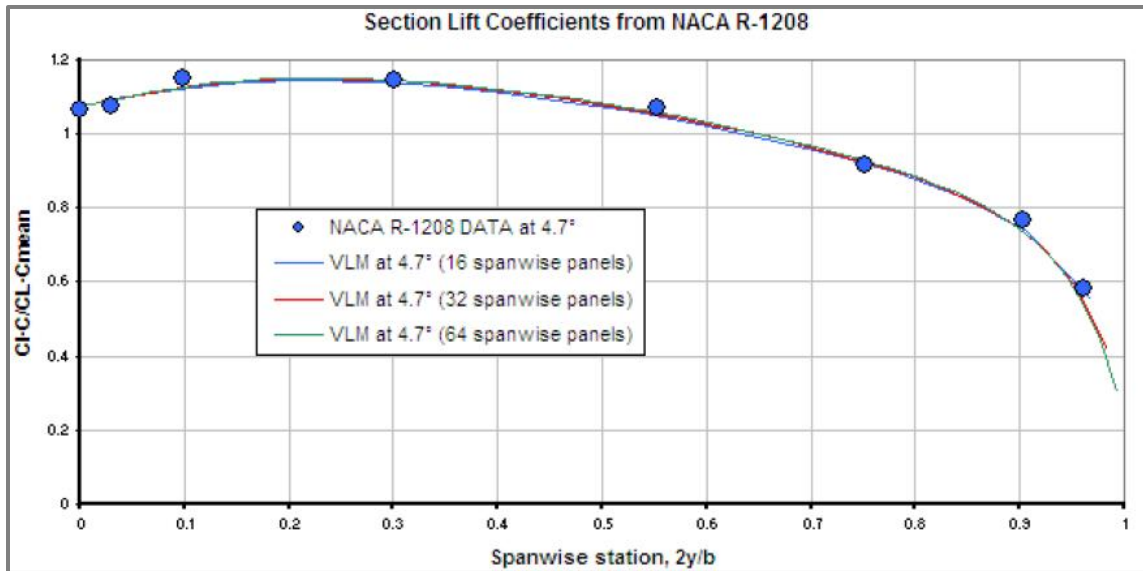


Figure C.1. SURFACES© Validation Example 1. The graph compares the lift coefficient over a swept back wing from NACA R-1208 to the predictions by SURFACES© at an AOA of 4.7° (Great OWL, 2009).

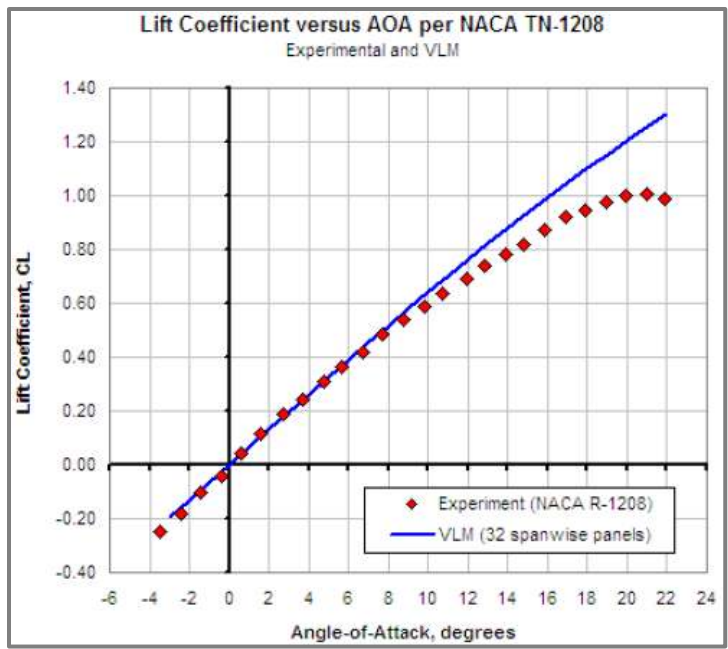


Figure C.2. SURFACES© Validation Example 2. Lift curve comparison between NACA R-1208 data and SURFACES© prediction. Visible is the absence of viscous effects at higher AOA, a limitation common to VLM programs (Great OWL, 2009).

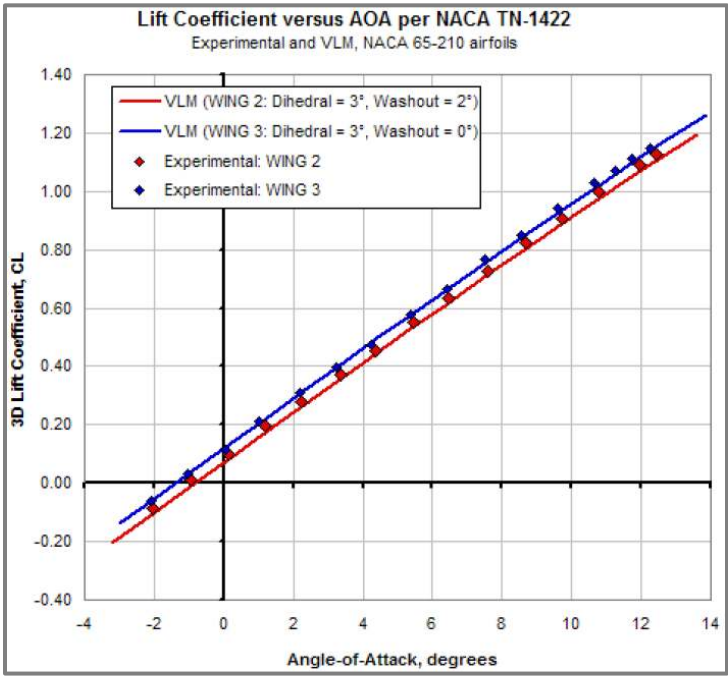


Figure C.3. SURFACES© Validation Example 3. The graph shows how SURFACES© takes into account the wash-out of an unswept, tapered wing (Great OWL, 2009).